Bending and twisting instabilities of columnar elliptical vortices in a rotating strongly stratified fluid

Paul Billant, D.G. Dritschel, Jean-Marc Chomaz

J. Fluid Mech. (2006), *vol.* 561, *pp.* 73–102.
doi:10.1017/S0022112006000516 Printed in the United Kingdom

Bending and twisting instabilities of columnar elliptical vortices in a rotating strongly stratified fluid

By PAUL BILLANT[1], DAVID G. DRITSCHEL[2] AND JEAN-MARC CHOMAZ[1]

[1]LadHyX, CNRS, École Polytechnique, F-91128 Palaiseau Cedex, France
[2]Mathematical Institute, University of St Andrews, St Andrews KY16 9SS, UK

(Received 15 December 2004 and in revised form 11 January 2006)

In this paper, we investigate the three-dimensional stability of the Moore–Saffman elliptical vortex in a rotating stratified fluid. By means of an asymptotic analysis for long vertical wavelength perturbations and small Froude number, we study the effects of Rossby number, external strain, and ellipticity of the vortex on the stability of azimuthal modes $m = 1$ (corresponding to a bending instability) and $m = 2$ (corresponding to a twisting instability).

In the case of a quasi-geostrophic fluid (small Rossby number), the asymptotic results are in striking agreement with previous numerical stability analyses even for vertical wavelengths of order one. For arbitrary Rossby number, the key finding is that the Rossby number has no effect on the domains of long-wavelength instability of these two modes: the two-dimensional or three-dimensional nature of the instabilities is controlled only by the background strain rate γ and by the rotation rate Ω of the principal axes of the elliptical vortex relative to the rotating frame of reference.

For the $m = 1$ mode, it is shown that when $\Omega < -\gamma$, the vortex is stable to any long-wavelength disturbances, when $-\gamma < \Omega \lesssim 0$, two-dimensional perturbations are most unstable, when $0 \lesssim \Omega < \gamma$, long-wavelength three-dimensional disturbances are the most unstable, and finally when $\gamma < \Omega$, short-wavelength three-dimensional perturbations are the most unstable. Similarly, the $m = 2$ instability is two-dimensional or three-dimensional depending only on γ and Ω, independent of the Rossby number. This means that if a long-wavelength three-dimensional instability exists for a given elliptical vortex in a quasi-geostrophic fluid, a similar instability should be observed for any other Rossby number, in particular for infinite Rossby number (strongly stratified fluids). This implies that the planetary rotation plays a minor role in the nature of the instabilities observed in rotating strongly stratified fluids.

The present results for the azimuthal mode $m = 1$ suggest that the vortex-bending instabilities observed previously in quasi-geostrophic fluids (tall-column instability) and in strongly stratified fluids (zigzag instability) are fundamentally related.

1. Introduction

Atmospheric and oceanic flows are strongly influenced by stable stratification and planetary rotation when the eddy turnover frequency U/L is small compared to the buoyancy frequency N and the rotation frequency Ω_b. This condition is met across a wide range of scales, but particularly at large scales. Because of the difference in order of magnitude between typical values of $N \approx 10^{-2} - 10^{-3}\,\mathrm{s}^{-1}$ and $\Omega_b \approx 10^{-4} - 10^{-5}\,\mathrm{s}^{-1}$

in the atmosphere and oceans at mid-latitudes, rotational effects tend to be more important at larger (horizontal) scales than stratification effects. In a broad range of scales (approximately 10–1000 km in the atmosphere, and 1–1000 km in the oceans), both effects act strongly, rendering motions layerwise two-dimensional with typical vertical/horizontal scale ratios of order $\Omega_b/N \ll 1$ (Dritschel, Ambaum & de la Torre Juárez 1999). In this range of scales, fluid motions are often described well by quasi-geostrophic dynamics. For an intermediate range of scales, rotational effects tend to be negligible while stratification effects are still dominant. In this non-rotating strongly stratified regime, the flow is also organized into thin layers (Riley & Lelong 2000) with a typical aspect ratio $U/NL \ll 1$, but with three-dimensional motions (Billant & Chomaz 2001; Lindborg 2002). A comprehensive study of atmospheric and oceanic dynamics, therefore, must take account of both the strongly stratified and the quasi-geostrophic regimes.

Dritschel & de la Torre Juárez (1996) have investigated the three-dimensional stability of vertical columnar elliptical vortices in a quasi-geostrophic fluid. They have shown that these vortices break down into three-dimensional vortices when their initial height to width aspect ratio exceeds about $6\Omega_b/N$. This breakdown is precipitated by a bending instability, called the 'tall-column instability', which predominantly displaces the vortex centreline.

In the case of a strongly stratified fluid without mean rotation ($\Omega_b = 0$), Billant & Chomaz (2000*a–c*) have also found an instability, called the 'zigzag instability', which vertically slices a columnar vortex pair into a sequence of shallow dipolar vortices with a thickness scaling like U/N.

Although the basic states considered in these two studies are different, both the tall-column instability and the zigzag instability appear to act similarly by bending columnar vortices and, ultimately, limiting their height. Here, we investigate whether these two instabilities have a similar physical origin.

To this end, the present work considers the three-dimensional instabilities of a single elliptical columnar vortex (the Moore–Saffman vortex) in a rotating strongly stratified fluid. Our primary goal is to determine the effect of the planetary rotation on the stability of this vortex, in order to relate the two instabilities previously described.

The three-dimensional stability of elliptical vortices in a quasi-geostrophic fluid has been investigated by Miyazaki & Hanazaki (1994), Dritschel & de la Torre Juárez (1996) and Miyazaki, Hirahara & Hanazaki (1997). Two types of instabilities may occur: long-(axial-)wavelength and short-wavelength instabilities. Miyazaki & Hanazaki (1994) and Miyazaki *et al*. (1997) have demonstrated that, for both types of instabilities, the physical mechanism can be understood as a resonance between inertial waves sustained by a weakly elliptical vortex and the rotating elliptical shape. This resonance occurs when the frequency of inertial waves matches the rotation rate of the strain field. The wavenumber of the resonance is given by the dispersion relation of the waves. Thus, the instability may be of the long-wavelength type if the background rotation matches the wave frequency for vanishing wavenumber, or of the short-wavelength type if this matching occurs for a wave with non-zero wavenumber. This physical mechanism resembles that of elliptic instability in homogeneous flows (Tsai & Widnall 1976; Pierrehumbert 1986; Waleffe 1990; Le Dizès & Eloy 1999; Kerswell 2002). An important difference, however, is that the quasi-geostrophic instabilities require a finite vortex core for their existence – the vortex boundary matters. Indeed, Miyazaki (1993) has demonstrated that no elliptic instability exists for an unbounded strained uniform vortex in a quasi-geostrophic fluid.

In this paper, we study the stability of the azimuthal modes $m = 1$ (corresponding to a bending instability) and $m = 2$ (corresponding to a twisting instability) by means of an asymptotic expansion for small vertical wavenumber. The advantage of this long-wavelength approach is that we can perform the analysis directly for any ellipticity, because the two-dimensional stability can be determined analytically (Love 1893; Moore & Saffman 1971). A similar long-wavelength stability analysis has been performed by Moore & Saffman (1971) for the $m = 1$ mode in a homogeneous fluid and in the particular case of a pure background strain. They have shown that long-wavelength three-dimensional effects are always stabilizing. In contrast, in the general case of a rotational background strain and in a strongly stratified fluid, we shall see that a rich behaviour can be predicted with three-dimensional effects stabilizing or destabilizing depending on the basic state, both for the $m = 1$ and $m = 2$ modes.

The paper is organized as follows. The stability problem is formulated in § 2: the governing equations are first given in § 2.1. The basic-state Moore–Saffman vortex is then described in § 2.2. The equations are non-dimensionalized in § 2.3 and linearized around the basic state in § 2.4. Finally, the boundary conditions are given in § 2.5. The stability results are described in § 3: the two-dimensional stability of the Moore–Saffman vortex is first briefly recalled in § 3.1, then the long-wavelength stability of the $m = 1$ and $m = 2$ modes are investigated in § 3.2 and § 3.3, respectively. Ideas for further work are discussed in § 4.

2. Stability problem

2.1. *Governing equations*

We consider a rotating stably stratified inviscid fluid under the Boussinesq approximation. The equations of momentum, continuity and density conservation read

$$\frac{\mathrm{D}\boldsymbol{u}}{\mathrm{D}t} + 2\Omega_b \boldsymbol{e}_z \times \boldsymbol{u} = -\frac{1}{\rho_0}\nabla p - \frac{g\rho'}{\rho_0}\boldsymbol{e}_z, \tag{2.1}$$

$$\nabla \cdot \boldsymbol{u} = 0, \tag{2.2}$$

$$\frac{\mathrm{D}\rho'}{\mathrm{D}t} + \frac{\partial \bar{\rho}}{\partial z} u_z = 0, \tag{2.3}$$

with $\boldsymbol{u}$ the velocity, Ω_b the rotation rate about the vertical axis, $\boldsymbol{e}_z$ the vertical unit vector, u_z the vertical velocity, p the pressure, and g the gravity. The total density field ρ has been decomposed as

$$\rho(\boldsymbol{x}, t) = \rho_0 + \bar{\rho}(z) + \rho'(\boldsymbol{x}, t), \tag{2.4}$$

with ρ_0 a constant reference density, $\bar{\rho}(z)$ a linear mean density profile and $\rho'(\boldsymbol{x}, t)$ a perturbation density. The density gradient defines the Brunt–Väisälä frequency $N = \sqrt{-(g/\rho_0)\partial\bar{\rho}/\partial z}$.

An important property of (2.1)–(2.3) is that they conserve the potential vorticity q following the motion

$$\frac{\mathrm{D}q}{\mathrm{D}t} = 0, \tag{2.5}$$

where

$$q = (2\Omega_b \boldsymbol{e}_z + \nabla \times \boldsymbol{u}) \cdot \left(\frac{\partial \bar{\rho}}{\partial z}\boldsymbol{e}_z + \nabla\rho' \right). \tag{2.6}$$

2.2. *The basic state*

We consider a basic state consisting of a vertical columnar elliptic vortex, having a uniform vorticity anomaly ζ, embedded in a uniform and unbounded pure straining flow whose principal axes rotate at rate Ω relative to the planetary reference frame rotating at rate Ω_b. A pure (i.e. without relative vorticity) straining flow in the planetary reference frame is chosen in order to model vortex interactions on a rotating planet for which the relative vorticity of the background straining flow is zero.

The major and minor semi-axes of the ellipse are denoted by a and b, respectively, and without loss of generality, we non-dimensionalize time and horizontal length by taking $\zeta = 1$ and $b = 1$. The absolute vorticity inside the elliptical vortex is therefore $1+2\Omega_b$, while the absolute vorticity of the straining flow is $2\Omega_b$. The latter is therefore not irrotational even though it is a pure strain.

The principal axes of the strain are steady in the reference frame rotating at rate $\Omega_b + \Omega$ relative to the inertial reference frame. In this new reference frame which we adopt hereinafter, the background straining flow is

$$u_x = (\Omega - \gamma)y, \quad u_y = -(\Omega + \gamma)x, \tag{2.7}$$

corresponding to a uniform strain γ with uniform relative background vorticity -2Ω (in the quasi-geostrophic limit studied by Dritschel & de la Torre Juárez (1996), Ω is negligible compared to Ω_b and hence $\Omega_b + \Omega$ can be approximated by Ω_b). As pointed out by Dritschel & de la Torre Juárez (1996) and explained in Appendix A, the straining flow (2.7) can be interpreted as the leading-order approximation of the flow induced by distant vortices surrounding the vortex under consideration. For example, in the case of the strain exerted by a distant vortex of the same intensity, we have $\Omega = 2\gamma$ if the surrounding vortex is of the same sign, and $\Omega = 0$ if the surrounding vortex is of the opposite sign.

An elliptical patch of uniform vorticity within the straining flow (2.7) is always an exact solution of the Euler equations, but the vortex aspect ratio $\lambda = a/b$ and orientation generally vary with time (Kida 1981). Moore & Saffman (1971) have shown that there exist solutions with constant aspect ratio when the angular velocity Ω of the principal axes is given by

$$\Omega = \frac{\lambda}{(\lambda+1)^2} - \gamma\frac{\lambda^2+1}{\lambda^2-1}. \tag{2.8}$$

Note that the rotation rate Ω_b of the planetary frame of reference does not enter into the above condition since the flow is two-dimensional and incompressible. It will come into play only in the three-dimensional stability analysis.

As shown in figure 1, for given values of the strain γ and background rotation Ω, there is either no solution, one or two solutions having different aspect ratios λ. These steady elliptical vortices are referred to as Moore–Saffman vortices (Moore & Saffman 1971). The particular case $\gamma = 0$, $\Omega = \lambda/(\lambda+1)^2$ corresponds to the Kirchhoff vortex. Note that we have represented only the solutions with $\lambda > 1$ since the solutions for $\lambda < 1$ can be deduced by means of the transformation $(x \to -y, y \to x, \gamma \to -\gamma)$.

In the frame of reference rotating at rate $\Omega_b + \Omega$ (the 'eigenframe' of the vortex), these solutions lie in elliptic or hyperbolic background straining flows with different orientations relative to the elliptical patch. In regions 1, 2 and 5 (figure 1), the background straining flow is elliptic since $|\Omega| > |\gamma|$. Its semi-major axis lies along the x-axis in regions 1 and 2 (figure 2*a*) whereas it lies along the y-axis in region 5

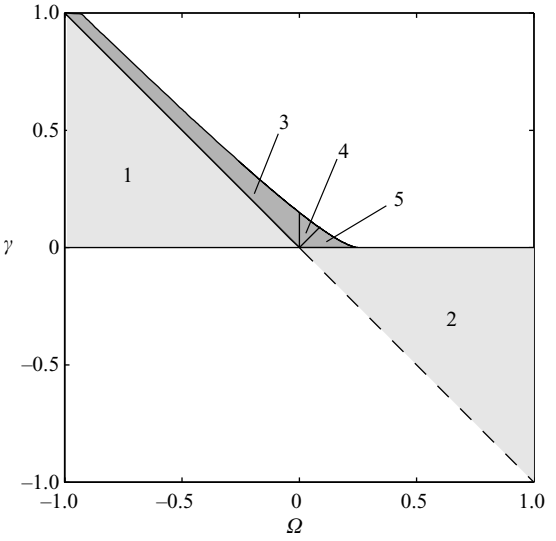

FIGURE 1. Domains of existence of the Moore–Saffman vortices with aspect ratio $\lambda > 1$. In the light and heavy shaded areas, there are one solution and two solutions, respectively. Steady solutions do not exist in the white areas or on the dashed line. The numbers correspond to the different streamline patterns shown in figure 2.

(figure 2*d*). The background straining flow is hyperbolic in regions 3 and 4. The strain axes make an angle smaller than $\pi/4$ in region 3 (figure 2*b*) and larger than $\pi/4$ in region 4 (figure 2*c*).

The streamfunction inside the Moore–Saffman vortex is given by

$$\psi_{0i} = \frac{1}{2}\left[\frac{1}{\lambda+1}(x^2+\lambda y^2) - (\Omega+\gamma)x^2 - (\Omega-\gamma)y^2\right], \tag{2.9}$$

where the streamfunction is defined by $u_{x0} = -\partial\psi_0/\partial y$, $u_{y0} = \partial\psi_0/\partial x$.

The exterior streamfunction is most conveniently written in a mixture of Cartesian coordinates (x, y, z) and elliptic-cylinder coordinates (ξ, η, z)

$$\psi_{0o} = \tfrac{1}{2}\lambda\xi + \tfrac{1}{4}\lambda e^{-2\xi}\cos 2\eta - \tfrac{1}{2}[(\Omega+\gamma)x^2 + (\Omega-\gamma)y^2], \tag{2.10}$$

where $x = c\cosh\xi\cos\eta$, $\quad y = c\sinh\xi\sin\eta$, $\quad 0 \leqslant \eta \leqslant 2\pi$ and $c = \sqrt{\lambda^2-1}$ is the focal semi-length of the ellipse. The last bracketed terms in (2.10) correspond to the uniform straining flow while the first terms correspond to the flow with zero relative vorticity which ensures velocity continuity at the boundary of the vortex.

In elliptic-cylinder coordinates, the boundary of the elliptical vortex is simply

$$\xi = \xi_0 = \tfrac{1}{2}\ln\left(\frac{\lambda+1}{\lambda-1}\right). \tag{2.11}$$

The Moore–Saffman vortex has uniform relative vertical vorticity ω_z, equal to $1-2\Omega$ and -2Ω inside and outside the ellipse, respectively (recall that the absolute vorticity is $1+2\Omega_b$ inside and $2\Omega_b$ outside). As for other vortex profiles (Moore & Saffman 1975), there is a difference between the strain rate inside and outside the ellipse: inside, the strain rate is uniform and equal to $\gamma+(\lambda-1)/2(\lambda+1)$ and outside, it tends towards γ at infinity.

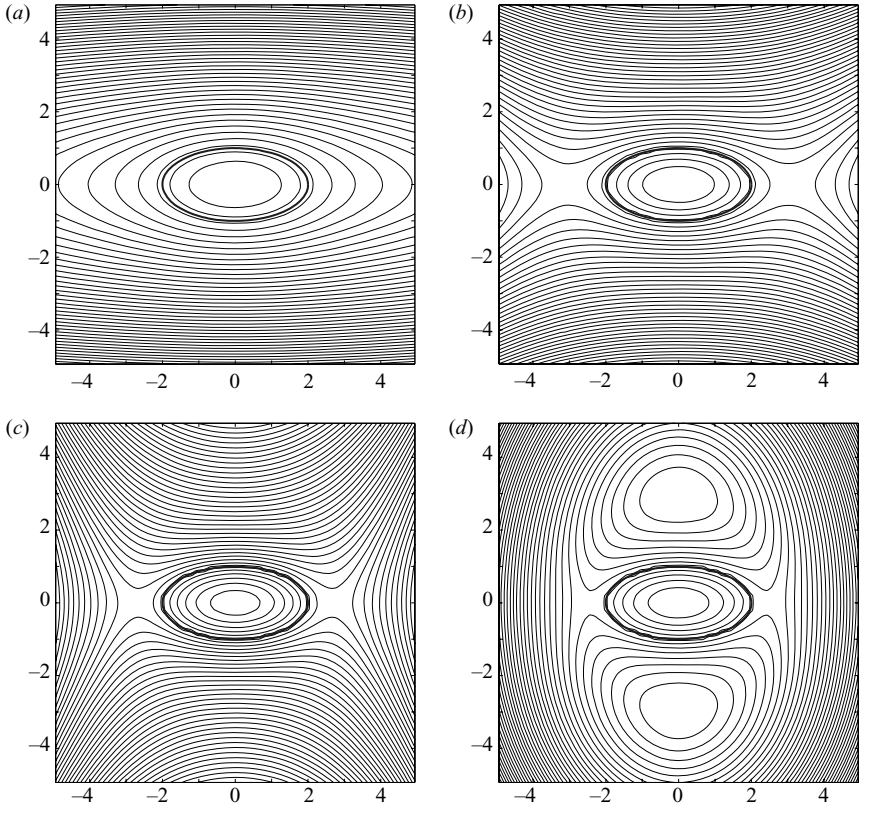

FIGURE 2. Streamlines of the Moore–Saffman elliptical vortex with aspect ratio $\lambda = 2$ for different values of the background vorticity Ω and strain rate γ. The bold line shows the boundary of the elliptical patch. (*a*) Elliptic background flow (region 1 of figure 1, $\Omega = -0.4$, $\gamma = 0.37$), (*b*) hyperbolic (region 3, $\Omega = -0.05$, $\gamma = 0.16$), (*c*) hyperbolic (region 4, $\Omega = 0.05$, $\gamma = 0.10$), (*d*) elliptic (region 5, $\Omega = 0.15$, $\gamma = 0.04$).

Finally, we remark that, even though we have chosen to consider a pure background straining flow relative to the planetary reference frame rotating at rate Ω_b, the case of a background straining flow with non-zero uniform relative vorticity ζ' in a reference frame rotating at rate Ω_b' can be deduced from our results simply by setting $\Omega_b = \Omega_b' + \zeta'/2$.

2.3. *Scaling analysis*

As stated in the previous section, horizontal length and time are non-dimensionalized such that the jump of vorticity across the boundary of the elliptical vortex is $\zeta = 1$ and the semi-minor axis of the ellipse is $b = 1$. We assume that the fluid is strongly stratified, i.e. the horizontal Froude number is small: $F_h = \zeta/N \ll 1$. Following Billant & Chomaz (2001), we take the vertical length scale to be the buoyancy length scale $L_v = \zeta b/N = 1/N$. The magnitude of the vertical velocity and density fluctuations are then $W = F_h \zeta b$ and $R = \rho_0 N \zeta b/g$, respectively.

With this scaling, equations (2.1)–(2.3) written in the reference frame rotating at rate $\Omega_b + \Omega$ (where the basic state is steady) become

$$\frac{\mathrm{D}\boldsymbol{u}_h}{\mathrm{D}t} + \left(\frac{1}{Ro} + 2\Omega\right)\boldsymbol{e}_z \times \boldsymbol{u}_h = -\nabla_h P, \tag{2.12}$$

$$F_h^2 \frac{\mathrm{D}u_z}{\mathrm{D}t} = -\frac{\partial P}{\partial z} - \rho', \tag{2.13}$$

$$\nabla \cdot \boldsymbol{u} = 0, \tag{2.14}$$

$$\frac{\mathrm{D}\rho'}{\mathrm{D}t} = u_z, \tag{2.15}$$

where the same notation has been kept for non-dimensional variables for simplicity and where ∇_h is the horizontal gradient, $P = p/\rho_0$ and $Ro = \zeta/2\Omega_b = 1/2\Omega_b$ is the Rossby number. The non-dimensional potential vorticity q becomes

$$q = \left(\frac{1}{Ro} + 2\Omega + \omega_z\right)\left(-1 + \frac{\partial \rho'}{\partial z}\right) + \left(F_h^2 \frac{\partial u_z}{\partial y} - \frac{\partial u_y}{\partial z}\right)\frac{\partial \rho'}{\partial x} - \left(F_h^2 \frac{\partial u_z}{\partial x} - \frac{\partial u_x}{\partial z}\right)\frac{\partial \rho'}{\partial y}, \tag{2.16}$$

where ω_z is the relative vertical vorticity. When the fluid is strongly stratified, $F_h \to 0$, hydrostatic balance can be assumed to hold in the vertical direction (2.13) and all terms in (2.16) involving F_h can be dropped.

2.4. *Linearized equations*

We subject the Moore–Saffman vortex (denoted by the subscript 0) to infinitesimal perturbations denoted by a tilde

$$(\boldsymbol{u}_h, u_z, P, \rho') = (\boldsymbol{u}_{h0}, 0, P_0, 0) + (\tilde{\boldsymbol{u}}_h, \tilde{u}_z, \tilde{P}, \tilde{\rho}')(\xi, \eta)\mathrm{e}^{\mathrm{i}kz+\sigma t}, \tag{2.17}$$

and linearize equations (2.12)–(2.15) with the approximation $F_h = 0$ to obtain governing equations for the disturbance quantities

$$\sigma \tilde{\boldsymbol{u}}_h + \left(Ro^{-1} + 2\Omega + \omega_{z0}\right)\boldsymbol{e}_z \times \tilde{\boldsymbol{u}}_h + \tilde{\omega}_z \boldsymbol{e}_z \times \boldsymbol{u}_{h0} + \nabla_h(\boldsymbol{u}_{h0} \cdot \tilde{\boldsymbol{u}}_h) = -\nabla_h \tilde{P}, \tag{2.18}$$

$$0 = -\mathrm{i}k\tilde{P} - \tilde{\rho}', \tag{2.19}$$

$$\nabla_h \cdot \tilde{\boldsymbol{u}}_h + \mathrm{i}k\tilde{u}_z = 0, \tag{2.20}$$

$$\sigma \tilde{\rho}' + \boldsymbol{u}_{h0} \cdot \nabla_h \tilde{\rho}' = \tilde{u}_z. \tag{2.21}$$

The potential vorticity of the perturbation is

$$\tilde{q} = (Ro^{-1} + 2\Omega + \omega_{z0})\mathrm{i}k\tilde{\rho}' - \tilde{\omega}_z, \tag{2.22}$$

where $\omega_{z0} = 1 - 2\Omega$ and -2Ω inside and outside the basic-state vortex. Note that $\tilde{q}$ is conserved following the basic motion since the potential vorticity of the basic state is piecewise constant:

$$\sigma \tilde{q} + \boldsymbol{u}_{h0} \cdot \nabla_h \tilde{q} = 0. \tag{2.23}$$

Because the perturbation has no potential vorticity initially, it is legitimate to assume that it remains zero for all time, i.e.

$$(Ro^{-1} + 2\Omega + \omega_{z0})\mathrm{i}k\tilde{\rho}' - \tilde{\omega}_z = 0. \tag{2.24}$$

This equation is more conveniently expressed using hydrostatic balance (2.19) and by decomposing the horizontal velocity into rotational and potential components with a streamfunction $\tilde{\psi}$ and a potential $\tilde{\chi}$

$$\tilde{\boldsymbol{u}}_h = -\nabla \times (\tilde{\psi}\boldsymbol{e}_z) + \nabla_h \tilde{\chi}. \tag{2.25}$$

Then, (2.24) becomes

$$\Delta_h \tilde{\psi} = k^2(Ro^{-1} + 2\Omega + \omega_{z0})\tilde{P}, \tag{2.26}$$

while the divergence equation (2.20) becomes

$$\Delta_h \tilde{\chi} = -k^2(\sigma \tilde{P} + \boldsymbol{u}_{h0} \cdot \nabla_h \tilde{P}). \tag{2.27}$$

These two equations of potential vorticity and mass conservation (2.26) and (2.27) together with the horizontal momentum equations (2.18) allow one to determine the solution in terms of $(\tilde{\psi}, \tilde{\chi}, \tilde{P})$.

2.5. *Boundary conditions*

We assume that the elliptical boundary is also distorted

$$\xi = \xi_0 + \tilde{\delta}(\eta)\mathrm{e}^{\mathrm{i}kz+\sigma t}. \tag{2.28}$$

The boundary conditions for the perturbations have been obtained by Moore & Saffman (1971). The kinematic boundary condition, which states that the boundary of the vortex continues to be the boundary, can be written at $\xi = \xi_0$

$$\tilde{u}_{\xi i} = \tilde{u}_{\xi o}, \tag{2.29}$$

$$\sigma h^2\tilde{\delta} + \Omega_e \frac{\partial h^2\tilde{\delta}}{\partial \eta} = h\tilde{u}_{\xi i}, \tag{2.30}$$

where

$$\Omega_e = (1-2\Omega)\frac{\lambda}{\lambda^2+1}. \tag{2.31}$$

and h^2 denotes the metric factor

$$h^2 = \tfrac{1}{2}c^2(\cosh 2\xi - \cos 2\eta), \tag{2.32}$$

while $c^2 = \lambda^2 - 1$. The dynamic condition at the boundary is the continuity of pressure which is equivalent to the continuity of tangential velocity (Moore & Saffman 1971)

$$h(\tilde{u}_{\eta o} - \tilde{u}_{\eta i}) = h^2\tilde{\delta} \quad \text{at} \quad \xi = \xi_o. \tag{2.33}$$

We also require that the disturbance decays as $\xi \to \infty$ and is non-singular at the vortex centre.

3. Stability analysis

3.1. *Two-dimensional stability*

Before tackling the three-dimensional stability problem, it is instructive to briefly recall the two-demensional stability results. The calculations may be carried out analytically as done by Love (1893) and Moore & Saffman (1971). Note that the Rossby and Froude numbers have no effect on two-dimensional perturbations since the Coriolis force derives from a potential in the case of pure two-dimensional perturbations and the buoyancy force acts only on three-dimensional perturbations.

Since the vorticity of the basic state is constant inside and outside the vortex, velocity perturbations in the two-dimensional case ($k = 0$) should have zero relative vertical vorticity everywhere (see (2.26)). We thus introduce potentials of the form

$$\tilde{\chi}_i = A\cosh m\xi\cos m\eta + B\sinh m\xi\sin m\eta \quad \text{for} \quad \xi < \xi_0, \tag{3.1}$$

$$\tilde{\chi}_o = \mathrm{e}^{-m\xi}(C_o\cos m\eta + D_o\sin m\eta) \quad \text{for} \quad \xi > \xi_0, \tag{3.2}$$

where (A, B, C_o, D_o) are constants and the velocity in elliptic-cylinder coordinates takes the form

$$\tilde{u}_\xi = \frac{1}{h}\frac{\partial\tilde{\chi}}{\partial\xi}, \quad \tilde{u}_\eta = \frac{1}{h}\frac{\partial\tilde{\chi}}{\partial\eta},$$

where h is the metric factor. The particular form of the potentials (3.1)–(3.2) is imposed by the boundary conditions at the vortex centre and at infinity. By enforcing the

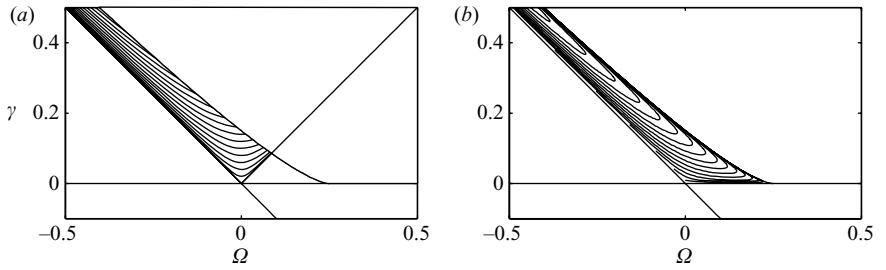

FIGURE 3. Growth rate of the (*a*) $m = 1$ and (*b*) $m = 2$ azimuthal modes in the two-dimensional case. The horizontal axis is Ω and the vertical axis is the strain γ. The contour interval is 0.02.

boundary conditions at $\xi = \xi_0$, Moore & Saffman (1971) have found the dispersion relation to be

$$\sigma^2 = \frac{1}{4}\left[\left(\frac{\lambda-1}{\lambda+1}\right)^{2m} - (2m\Omega_e - 1)^2\right]. \tag{3.3}$$

When $m = 1$, this reduces to

$$\sigma^2 = \gamma^2 - \Omega^2, \tag{3.4}$$

where Ω is related to γ and λ through (2.8). Thus, the mode $m = 1$ is unstable when the background straining flow is hyperbolic: $|\gamma| > |\Omega|$. As seen in figure 3(*a*), this occurs over almost the entire domain where two steady solutions exist. According to Moore & Saffman (1971), this instability corresponds merely to a drift of the vortex without change of shape and cannot be considered a true instability. When $\gamma = 0$, the $m = 1$ mode is neutral with a frequency $\sigma = \pm i\Omega$, because of translational invariance.

When $m = 2$, we have

$$\sigma^2 = 4\gamma\lambda\frac{\lambda-1}{(\lambda+1)^3} - 16\gamma^2\frac{\lambda^2}{(\lambda^2-1)^2}. \tag{3.5}$$

As shown in figure 3(*b*), the $m = 2$ mode is unstable over the entire domain where there are two steady solutions. However, only the solution with the largest aspect ratio is unstable to $m = 2$ disturbances – the other solution is stable. Note that the $m = 2$ mode is neutral when $\gamma = 0$, because of rotational invariance, i.e. because the orientation of the ellipse is arbitrary.

Another interesting way of looking at these two-dimensional instabilities is in the (Ω, λ) parameter space. In figure 4, we see that each azimuthal mode has a tongue of instability which erupts from $\lambda = 1$ at $\Omega = (1/2)(1 - 1/m)$. In the limit $\lambda \to 1$, instability occurs when the background rotation Ω matches the frequency of two-dimensional inertial (or Kelvin) waves on a circular vortex with unit vorticity. These instabilities can therefore be interpreted as an unstable resonance when the strain rotates at the same angular velocity as the mth azimuthal mode.

3.2. *Long-wavelength instability of the $m = 1$ mode*

When the vertical wavenumber is small $k \ll 1$, it is tempting to perform a straightforward asymptotic analysis by expanding perturbations in k, for example,

$$\tilde{\boldsymbol{u}}_h = \tilde{\boldsymbol{u}}_{h0} + k^2\tilde{\boldsymbol{u}}_{h2} + k^4\tilde{\boldsymbol{u}}_{h4} + \cdots, \tag{3.6}$$

where $\tilde{\boldsymbol{u}}_{h0}$ is the two-dimensional velocity perturbation calculated in the previous section. Each order could then be determined by inserting the expansion (3.6) into the

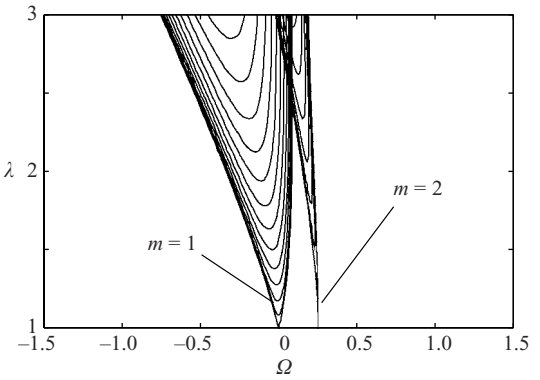

FIGURE 4. Growth rate of the $m = 1$ and $m = 2$ azimuthal modes in the two-dimensional case. The contour interval is 0.02.

linearized equations (2.18), (2.26) and (2.27) and by solving order by order in k. However, far from the vortex centre, i.e. when $x \gg 1$ or $y \gg 1$, we have $kx \approx O(1)$ or $ky \approx O(1)$ and horizontal and vertical derivatives become of the same order. It appears that some terms which would be neglected by the naïve expansion (3.6) become dominant in this region.

We must therefore divide the exterior region into two regions: the inner region where $x, y \approx O(1)$ and $k \ll 1$, and the outer region where $kx, ky \approx O(1)$ together with $k \ll 1$ and perform a matching between these two regions. For the $m = 1$ mode, we shall see that these two expansions can be matched only if we include, in the inner perturbation, a term scaling as $k^2 \ln k$, for example for the horizontal velocity

$$\tilde{\boldsymbol{u}}_{ho} = \tilde{\boldsymbol{u}}_{ho0} + k^2 \ln k \, \tilde{\boldsymbol{u}}_{ho2a} + k^2 \tilde{\boldsymbol{u}}_{ho2b} + \cdots. \tag{3.7}$$

Because there is no term $k^2 \ln k$ in the linearized equations (2.18), (2.26) and (2.27), the solution $\tilde{\boldsymbol{u}}_{ho2a}$ is necessarily a homogeneous solution of the two-dimensional problem, i.e. $\tilde{\boldsymbol{u}}_{ho2a} = \nabla_h \tilde{\chi}_{o2a}$ with

$$\tilde{\chi}_{o2a} = C_2 \cosh\xi \cos\eta + D_2 \sinh\xi \sin\eta. \tag{3.8}$$

Such a term which is forced by the matching condition from the outer region is sometimes called a switchback (Hinch 1991). Without loss of generality, it is not necessary to include terms of the form $\sinh\xi \cos\eta$ or $\cosh\xi \sin\eta$ in (3.8) since they can be eliminated by a simple rescaling of the leading-order two-dimensional solution. It is also noteworthy that we are fully allowed to have functions of the form e^{ξ} in the inner region because, as we shall see below, these functions can be matched with decreasing functions of ξ in the outer region. In other words, the form of (3.8) is not inconsistent with the requirement that disturbances decay at infinity.

It may be noticed that a term scaling as $k^2 \ln k$ is also present in the long-wavelength stability analysis of the $m = 1$ mode of Moore & Saffman (1971) in a homogeneous fluid and for a pure strain $\Omega = 0$. In their case, the exterior perturbation is a potential flow and can be directly found in terms of Mathieu functions. Here, in a rotating stratified fluid, the exterior perturbation is more difficult to find because it is not a potential flow.

3.2.1. *Interior and inner exterior regions*

We first determine the interior and inner exterior perturbations. In this section, a regular expansion is assumed for both solutions

$$\tilde{\boldsymbol{u}}_h = \tilde{\boldsymbol{u}}_{h0} + k^2\tilde{\boldsymbol{u}}_{h2} + \cdots, \tag{3.9}$$

$$\tilde{P} = \tilde{P}_0 + k^2\tilde{P}_2 + \cdots, \tag{3.10}$$

$$\tilde{\chi} = \tilde{\chi}_0 + k^2\tilde{\chi}_2 + \cdots, \tag{3.11}$$

$$\tilde{\psi} = k^2\tilde{\psi}_2 + \cdots, \tag{3.12}$$

and directly inserted into (2.18), (2.26) and (2.27). The non-trivial terms mentioned in § 3.2 will be added to the inner exterior solution later and determined by matching with the outer exterior solution.

In what follows, it proves convenient to introduce the parameters

$$\alpha_j = Ro^{-1} - j\Omega, \tag{3.13}$$

$j = 1$, 2 and 4, which depend only on the basic state. These occur frequently below.

The potentials at order zero are two-dimensional

$$\tilde{\chi}_{i0} = A\cosh\xi\cos\eta + B\sinh\xi\sin\eta \quad \text{for} \quad \xi < \xi_0, \tag{3.14}$$

$$\tilde{\chi}_{o0} = \mathrm{e}^{-\xi}(C_o\cos\eta + D_o\sin\eta) \quad \text{for} \quad \xi > \xi_0, \tag{3.15}$$

and $\tilde{\psi}_0$ has been set to zero since the perturbation has zero relative vertical vorticity in the two-dimensional limit. The pressure at order zero is first determined from the horizontal momentum equation (2.18). This equation can be easily integrated because $\omega_{z0} = const$ and $\Delta_h\tilde{\chi}_0 = 0$

$$\tilde{P}_0 = -\sigma\tilde{\chi}_0 + (\omega_{z0} + Ro^{-1} + 2\Omega)\tilde{\chi}_{c0} - \boldsymbol{u}_{h0}\cdot\nabla_h\tilde{\chi}_0, \tag{3.16}$$

where $\tilde{\chi}_{c0}$ is the streamfunction corresponding to the potential $\tilde{\chi}_0$:

$$\frac{\partial\tilde{\chi}_{c0}}{\partial\xi} = \frac{\partial\tilde{\chi}_0}{\partial\eta}, \quad \frac{\partial\tilde{\chi}_{c0}}{\partial\eta} = -\frac{\partial\tilde{\chi}_0}{\partial\xi}. \tag{3.17}$$

The explicit form of the pressure in the interior and the exterior is

$$\begin{aligned}\tilde{P}_{i0} = &\left[-\sigma A + B\left(\frac{1}{Ro} + \Omega + \gamma + \frac{\lambda}{\lambda+1}\right)\right]\cosh\xi\cos\eta \\ &- \left[\sigma B + A\left(\frac{1}{Ro} + \Omega - \gamma + \frac{1}{\lambda+1}\right)\right]\sinh\xi\sin\eta \quad \text{for} \quad \xi < \xi_0,\end{aligned} \tag{3.18}$$

$$\begin{aligned}\tilde{P}_{o0} = &\left[D_o\left(H(\xi) + \frac{f(\xi)}{h^2}\sinh\xi\right) - C_o\sigma e^{-\xi}\right]\cos\eta \\ &- \left[C_o\left(H(\xi) + \frac{f(\xi)}{h^2}\cosh\xi\right) + D_o\sigma e^{-\xi}\right]\sin\eta \quad \text{for} \quad \xi > \xi_0,\end{aligned} \tag{3.19}$$

where $H(\xi) = -(Ro^{-1} + \Omega)\mathrm{e}^{-\xi} - \gamma\mathrm{e}^{\xi}$ and $f(\xi) = -\lambda\mathrm{e}^{-2\xi} + c^2(\Omega + \gamma\cosh 2\xi)$.

Then, knowing the pressure at order zero, we can compute $\tilde{\psi}_2$ from (2.26)

$$\Delta_h\tilde{\psi}_2 = (Ro^{-1} + 2\Omega + \omega_{z0})\tilde{P}_0. \tag{3.20}$$

The interior solution is of the form

$$\tilde{\psi}_{i2} = (a_1A + a_2B)\cosh^3\xi\left(\cos\eta + \tfrac{1}{3}\cos 3\eta\right) + (a_3A + a_1B)\sinh^3\xi\left(\sin\eta - \tfrac{1}{3}\sin 3\eta\right), \tag{3.21}$$

where the coefficients (a_1, a_2, a_3) are given in Appendix B. Similarly, the exterior solution can be written

$$\tilde{\psi}_{o2} = (C_o H_1(\xi) + D_o H_2(\xi)) \cos\eta + (C_o H_3(\xi) + D_o H_4(\xi)) \sin\eta + \psi_{o23c}(\xi) \cos 3\eta + \psi_{o23s}(\xi) \sin 3\eta. \tag{3.22}$$

The functions H_1, H_2, H_3 and H_4 introduced in (3.22) are also defined in Appendix B. The functions $\psi_{o23c}(\xi)$ and $\psi_{o23s}(\xi)$ will not be required in the sequel.

Then $\tilde{\chi}_2$ is obtained from (2.27)

$$\Delta_h \tilde{\chi}_2 = -\sigma \tilde{P}_0 - \boldsymbol{u}_{h0} \cdot \nabla_h \tilde{P}_0. \tag{3.23}$$

Inside, we have

$$\tilde{\chi}_{i2} = (b_1 A + b_2 B) \cosh^3\xi \left(\cos\eta + \tfrac{1}{3}\cos 3\eta\right) + (b_3 A + b_4 B) \sinh^3\xi \left(\sin\eta - \tfrac{1}{3}\sin 3\eta\right), \tag{3.24}$$

where (b_1, b_2, b_3, b_4) are given in Appendix B. Outside, equation (3.23) is more difficult to solve analytically because its right-hand side multiplied by h^2 contains some terms with the metric factor h^2 in their denominator. Writing these terms as infinite Fourier series, it is, however, possible to find the solution of (3.23) analytically in the form:

$$\tilde{\chi}_{o2} = (G_1(\xi) C_o + G_2(\xi) D_o) \cos\eta + (G_3(\xi) C_o + G_4(\xi) D_o) \sin\eta + \chi_{o23c} \cos 3\eta + \chi_{o23s} \sin 3\eta + \chi_{o25c} \cos 5\eta + \chi_{o25s} \sin 5\eta + \cdots. \tag{3.25}$$

Only the functions G_1, G_2, G_3 and G_4, defined in Appendix B, are required to compute the boundary conditions at $\xi = \xi_0$ for the azimuthal component $m = 1$.

3.2.2. *Outer exterior region*

The inner exterior solution is not uniformly valid: as can be seen from the functions $H_i(\xi)$ and $G_i(\xi)$ (Appendix B), the streamfunction $\tilde{\psi}_{o2}$ and potential $\tilde{\chi}_{o2}$ do not decay, but grow as $\xi \exp\xi$ for large ξ. The goal of this section is to find a uniformly valid solution at large distances from the vortex.

As shown previously, the horizontal momentum equation (2.18) can be easily integrated in the two-dimensional limit ($k = 0$) because $\omega_{z0} = const$ and $\Delta_h \tilde{\psi} = 0$, $\Delta_h \tilde{\chi} = 0$. This gives the pressure in the form

$$\tilde{P}_0 = -\sigma(\tilde{\chi} + \tilde{\psi}_c) + (Ro^{-1} + 2\Omega + \omega_{z0})(\tilde{\psi} + \tilde{\chi}_c) - \tilde{\boldsymbol{u}}_h \cdot \boldsymbol{u}_{h0}, \tag{3.26}$$

where $\nabla_h \tilde{\psi}_c = -\nabla \times (\tilde{\psi} \boldsymbol{e}_z)$ and $\nabla \times (\tilde{\chi}_c \boldsymbol{e}_z) = -\nabla_h \tilde{\chi}$.

In the three-dimensional case for small wavenumber $k \ll 1$, the pressure will be

$$\tilde{P} = \tilde{P}_0 + O(k^2 \ln k), \tag{3.27}$$

with now $\nabla_h \tilde{\psi}_c = -\nabla \times (\tilde{\psi} \boldsymbol{e}_z) + O(k^2 \ln k)$, $\nabla \times (\tilde{\chi}_c \boldsymbol{e}_z) = -\nabla_h \tilde{\chi} + O(k^2 \ln k)$. Inserting this approximate solution for the pressure into (2.26) and (2.27) gives

$$\Delta_h \tilde{\psi} = k^2 (Ro^{-1} + 2\Omega + \omega_{z0}) \tilde{P}_0 + O(k^4 \ln k), \tag{3.28}$$

and

$$\Delta_h \tilde{\chi} = -k^2 (\sigma \tilde{P}_0 + \boldsymbol{u}_{h0} \cdot \nabla_h \tilde{P}_0) + O(k^4 \ln k), \tag{3.29}$$

where $\tilde{P}_0$ should be substituted by (3.26). The way to obtain a uniformly valid solution is to solve these two approximate equations as a whole, instead of doing an expansion in k as in the inner exterior region. In this way, we shall see that we can obtain a uniformly valid solution at large distances from the vortex and valid up to $O(k^2 \ln k)$.

The first step is to further simplify these equations because we need only the solution at large distances from the vortex. Using cylindrical coordinates $(s,\ \theta)$ with $x = s\cos\theta$ and $y = s\sin\theta$, then at large radius s, the exterior basic streamfunction (2.10) tends to the uniform straining flow

$$\psi_{0o} = -\tfrac{1}{2}(\Omega s^2 + \gamma s^2 \cos 2\theta) + O(\ln s). \tag{3.30}$$

It is important to remark that even if γ and Ω are very small, the straining flow is always dominant for large radius because its streamfunction varies as s^2, while the streamfunction due to the vortex itself varies as $\ln s$ and therefore becomes negligible for large s. Hence the outer solution cannot be found by an asymptotic expansion in Ω and γ, even if they happen to be small.

The pressure in the two-dimensional limit becomes

$$\begin{aligned}\tilde{P}_0 = -\sigma(\tilde{\chi} + \tilde{\psi}_c) + \frac{1}{Ro}(\tilde{\psi} + \tilde{\chi}_c) + (\Omega + \gamma\cos 2\theta)\left(\frac{\partial\tilde{\chi}}{\partial\theta} + s\frac{\partial\tilde{\psi}}{\partial s}\right)\\ - \gamma\sin 2\theta\left(\frac{\partial\tilde{\psi}}{\partial\theta} - s\frac{\partial\tilde{\chi}}{\partial s}\right) + O(1/s^2),\end{aligned} \tag{3.31}$$

and (3.28) and (3.29) become

$$\Delta_h\tilde{\psi} = k^2 Ro^{-1}\tilde{P}_0 + O(k^4\ln k), \tag{3.32}$$

$$\Delta_h\tilde{\chi} = -k^2\left(\sigma\tilde{P}_0 + \Omega\frac{\partial\tilde{P}_0}{\partial\theta} + \gamma\cos 2\theta\frac{\partial\tilde{P}_0}{\partial\theta} + \gamma\sin 2\theta\, s\frac{\partial\tilde{P}_0}{\partial s}\right) + O\left(\frac{k^2}{s^2}, k^4\ln k\right). \tag{3.33}$$

At this level of approximation, we can also consider only the first modes of $\tilde{\chi}$ and $\tilde{\psi}$

$$\tilde{\chi} = \tilde{\chi}_+(s)\mathrm{e}^{\mathrm{i}\theta} + \tilde{\chi}_-(s)\mathrm{e}^{-\mathrm{i}\theta} + \cdots, \tag{3.34}$$

$$\tilde{\psi} = \tilde{\psi}_+(s)\mathrm{e}^{\mathrm{i}\theta} + \tilde{\psi}_-(s)\mathrm{e}^{-\mathrm{i}\theta} + \cdots, \tag{3.35}$$

written using exponentials instead of sine and cosine functions for simplicity. Terms associated with higher azimuthal wavenumbers such as $\mathrm{e}^{\pm 3\mathrm{i}\theta}$ are at most $O(k^2\ln k)$ and appear at $O(k^4\ln k)$ on the right-hand sides of (3.32) and (3.33). Moreover, they are not necessary for the matching of the $m = 1$ mode. We have also

$$\tilde{\psi}_{c+} = -\mathrm{i}s\frac{\partial\tilde{\psi}_+}{\partial s} + O(k^2\ln k), \quad \tilde{\chi}_{c+} = \mathrm{i}s\frac{\partial\tilde{\chi}_+}{\partial s} + O(k^2\ln k).$$

All these simplifications inserted into (3.32) and (3.33) give

$$\begin{aligned}\Delta_h\tilde{\psi}_+ = \frac{k^2}{Ro}\left[-\left(S + \frac{\mathrm{i}}{Ro}\right)(\tilde{\chi}_+ + \mathrm{i}\tilde{\psi}_+) + \mathrm{i}S\frac{\partial s\tilde{\psi}_+}{\partial s} + \frac{\mathrm{i}}{Ro}\frac{\partial s\tilde{\chi}_+}{\partial s} + \frac{\gamma}{2}\frac{\partial}{\partial s}s(\tilde{\psi}_- - \mathrm{i}\tilde{\chi}_-)\right]\\ + O\left(\frac{k^2}{s^2}, k^4\ln k\right),\end{aligned} \tag{3.36}$$

$$\begin{aligned}\Delta_h\tilde{\chi}_+ = k^2\left[\left(S^2 + \frac{\mathrm{i}S}{Ro} - \gamma^2\right)(\tilde{\chi}_+ + \mathrm{i}\tilde{\psi}_+) - \mathrm{i}S^2\frac{\partial s\tilde{\psi}_+}{\partial s} - \frac{\mathrm{i}S}{Ro}\frac{\partial s\tilde{\chi}_+}{\partial s} + \frac{\gamma^2}{2}\frac{\partial}{\partial s}\left(s\frac{\partial s\tilde{\chi}_+}{\partial s}\right)\right.\\ \left. + \mathrm{i}\gamma\sigma\frac{\partial s\tilde{\chi}_-}{\partial s} - \frac{\gamma}{2Ro}s\frac{\partial^2 s\tilde{\chi}_-}{\partial s^2} - \frac{\gamma}{2}\left(S + \frac{\mathrm{i}}{Ro}\right)\frac{\partial s\tilde{\psi}_-}{\partial s} - \frac{\gamma}{2}(S + 2\mathrm{i}\Omega)s\frac{\partial^2 s\tilde{\psi}_-}{\partial s^2}\right]\\ + O\left(\frac{k^2}{s^2}, k^4\ln k\right),\end{aligned} \tag{3.37}$$

where $S = \sigma - \mathrm{i}\Omega$. The equations for $\tilde{\chi}_-$ and $\tilde{\psi}_-$ are the same, but with complex conjugate coefficients. All the derivatives appearing on the right-hand sides of these equations can be further neglected up to order k^2 because

$$\frac{\partial s\tilde{\chi}_\pm}{\partial s} = O(k^2 \ln k), \quad \frac{\partial s\tilde{\psi}_\pm}{\partial s} = O(k^2 \ln k).$$

Upon defining a stretched radius $r = sk$, such that $r = O(1)$, these additional simplifications finally yield

$$\Delta_h \tilde{\psi}_+ = -Ro^{-1}(S + \mathrm{i}Ro^{-1})(\tilde{\chi}_+ + \mathrm{i}\tilde{\psi}_+) + O(k^2 \ln k), \tag{3.38}$$

$$\Delta_h \tilde{\chi}_+ = (S^2 + \mathrm{i}Ro^{-1}S - \gamma^2)(\tilde{\chi}_+ + \mathrm{i}\tilde{\psi}_+) + O(k^2 \ln k). \tag{3.39}$$

The same notation has been kept for the Laplacian Δ_h in term of the streched radius r. The terms of $O(1/s^2) \approx O(k^2)$ are now included in the neglected terms of $O(k^2 \ln k)$. This means that only the uniform straining flow of the basic flow is indeed required for solving the outer problem at order $O(k^2 \ln k)$. The solution can then be easily found:

$$\tilde{\chi}_+ = Ek\tilde{\beta}(S(S + \mathrm{i}Ro^{-1}) - \gamma^2)K_1(\tilde{\beta}r)(1 + O(k^2 \ln k)) - \frac{\mathrm{i}Fk}{r}, \tag{3.40}$$

$$\tilde{\psi}_+ = -Ek\tilde{\beta}Ro^{-1}(S + \mathrm{i}Ro^{-1})K_1(\tilde{\beta}r)(1 + O(k^2 \ln k)) + \frac{Fk}{r}, \tag{3.41}$$

where $\tilde{\beta}^2 = S^2 + Ro^{-2} - \gamma^2$, (E, F) are constants and K_1 is the modified Bessel function of the second kind of order one (note that the sign of the real part of $\tilde{\beta}$ is chosen as positive). This solution is uniformly valid for large distances $r = O(1)$ at order $O(k^2 \ln k)$: it decays for large radius and tends to $1/r$ for small radius. It is also noteworthy that when $\gamma = 0$ and when $\psi_{0o} = -\Omega s^2/2$ exactly, the above solution is exact. When $Ro \ll (1/\Omega, 1/\gamma)$, we also recover the quasi-geostrophic solution $\tilde{\psi}_+ \propto K_1(r/Ro)$ for which $\tilde{\chi}_+ \ll \tilde{\psi}_+$.

3.2.3. *Matching between the inner and outer exterior solutions*

To match the inner and outer exterior solutions, it is first necessary to add arbitrary two-dimensional (homogeneous) solutions $\propto k^2 \ln k$ and k^2 to the inner exterior solutions $\tilde{\psi}_o$ and $\tilde{\chi}_o$ obtained at order k^2 in § 3.2.1:

$$\begin{aligned}\tilde{\chi}_o = {} & \tilde{\chi}_{o0} + k^2\tilde{\chi}_{o2} + k^2(C_2 \ln k + C_3)\cosh\xi\cos\eta \\ & + k^2(D_2 \ln k + D_3)\sinh\xi\sin\eta + O(k^4 \ln k),\end{aligned} \tag{3.42}$$

$$\begin{aligned}\tilde{\psi}_o = {} & k^2\tilde{\psi}_{o2} + k^2(L_2 \ln k + L_3)\cosh\xi\cos\eta \\ & + k^2(M_2 \ln k + M_3)\sinh\xi\sin\eta + O(k^4 \ln k).\end{aligned} \tag{3.43}$$

The constants $(C_2, C_3, D_2, D_3, L_2, L_3, M_2, M_3)$ will be determined by matching with the outer solution. As noted previously, it is not necessary to add free solutions of the form $\sinh\xi\cos\eta$ or $\cosh\xi\sin\eta$ because they can be eliminated at order $O(k^4 \ln k)$ by a simple rescaling of the two-dimensional solution $\tilde{\chi}_{o0}$. To perform the matching, we introduce an intermediate radius τ covering the overlap region between the inner and outer regions. Its definition in terms of the inner variables is

$$\tau\cos\theta = k^\phi c\cosh\xi\cos\eta, \quad \tau\sin\theta = k^\phi c\sinh\xi\sin\eta, \tag{3.44}$$

while, in terms of the outer radius r defined in (3.40)–(3.41), we have $\tau = rk^{\phi-1}$. The parameter ϕ allows us to switch from the inner expansion for $\phi = 0$ to the outer expansion for $\phi = 1$. In the intermediate region $0 < \phi < 1$, both expansions should

match. We re-express the inner and outer exterior solutions in terms of τ and consider the limit $\tau = O(1)$ together with $k \ll 1$. For the inner elliptic cylinder coordinates, this implies $e^{\xi} = (2/k^{\phi}c)(\tau + O(k^{2\phi}))$ and $\eta = \theta(1 + O(k^{2\phi}))$. Replacing ξ and η in (3.42)–(3.43) by these expressions and writing the potential and the streamfunction in the form

$$\tilde{\chi}_o = \tilde{\chi}_{o+}(\tau)e^{i\theta} + \tilde{\chi}_{o-}(\tau)e^{-i\theta} + \cdots,$$
$$\tilde{\psi}_o = \tilde{\psi}_{o+}(\tau)e^{i\theta} + \tilde{\psi}_{o-}(\tau)e^{-i\theta} + \cdots,$$

gives at leading orders

$$\tilde{\chi}_{o+} = k^{\phi}\frac{c}{4\tau}(C_o - iD_o) + k^{2-\phi}\frac{\tau c}{8}\ln\left(\frac{2\tau}{k^{\phi}c}\right)(S(S + iRo^{-1}) - \gamma^2)(C_o - iD_o)$$
$$+ k^{2-\phi}\frac{\tau}{2c}((C_2 - iD_2)\ln k + C_3 - iD_3) + O(k^{2+\phi}\ln k), \tag{3.45}$$
$$\tilde{\psi}_{o+} = -k^{2-\phi}\frac{\tau c}{8}\ln\left(\frac{2\tau}{k^{\phi}c}\right)Ro^{-1}(S + iRo^{-1})(C_o - iD_o)$$
$$+ k^{2-\phi}\frac{\tau}{2c}((L_2 - iM_2)\ln k + L_3 - iM_3) + O(k^{2+\phi}\ln k). \tag{3.46}$$

The outer solution (3.40)–(3.41) becomes

$$\tilde{\chi}_{+} = E(S(S + iRo^{-1}) - \gamma^2)\left[\frac{k^{\phi}}{\tau} + \frac{\tilde{\beta}^2\tau k^{2-\phi}}{2}\left(\ln\left(\frac{\tilde{\beta}\tau k^{1-\phi}}{2}\right) + C - \frac{1}{2}\right)\right]$$
$$- \frac{iFk^{\phi}}{\tau} + O(k^3\ln k, k^{4-3\phi}\ln k), \tag{3.47}$$
$$\tilde{\psi}_{+} = -ERo^{-1}(S + iRo^{-1})\left[\frac{k^{\phi}}{\tau} + \frac{\tilde{\beta}^2\tau k^{2-\phi}}{2}\left(\ln\left(\frac{\tilde{\beta}\tau k^{1-\phi}}{2}\right) + C - \frac{1}{2}\right)\right]$$
$$+ \frac{Fk^{\phi}}{\tau} + O(k^3\ln k, k^{4-3\phi}\ln k), \tag{3.48}$$

where $C = 0.5772\ldots$ is Euler's constant. We may remark that the outer solution found at order $O(k^3\ln k)$ in the previous section is sufficient for the matching since the order of the inner solution is $O(k^{\phi+2}\ln k)$ with $0 < \phi < 1$.

The inner (3.45)–(3.46) and outer (3.47)–(3.48) exterior solutions have similar dependence on the intermediate radius τ. They are identical regardless of the value of ϕ if we set

$$E = \frac{c}{4\tilde{\beta}^2}(C_o - iD_o), \quad F = \frac{E}{Ro}\left(S + \frac{i}{Ro}\right), \tag{3.49}$$

and the constants $(C_2, D_2, C_3, D_3, L_2, M_2, L_3, M_3)$ as functions of (C_o, D_o) are defined in Appendix B.

3.2.4. *Dispersion relation*

We have now completely determined uniformly valid solutions up to order k^2 so that we can repeat the calculation of the growth rate, replacing (3.1) by (3.11)–(3.12) and (3.2) by (3.42)–(3.43), and imposing the same boundary conditions (2.29)–(2.30)–(2.33). This leads to the following dispersion relation

$$\left[\sigma - \tfrac{1}{2}\lambda\sigma\alpha_1 k^2\ln\kappa + \tfrac{1}{4}\lambda(\gamma^2 - \sigma^2 + \alpha_1^2)k^2\arg\tilde{\beta} - \sigma\Gamma_1 k^2\right]^2$$
$$+\left[\Omega + \tfrac{1}{4}\lambda(\gamma^2 - \sigma^2 + \alpha_1^2)k^2\ln\kappa + \tfrac{1}{2}\lambda\sigma\alpha_1 k^2\arg\tilde{\beta} + \Gamma_2 k^2\right]^2 = (\gamma + \Gamma_3 k^2)^2\,, \tag{3.50}$$

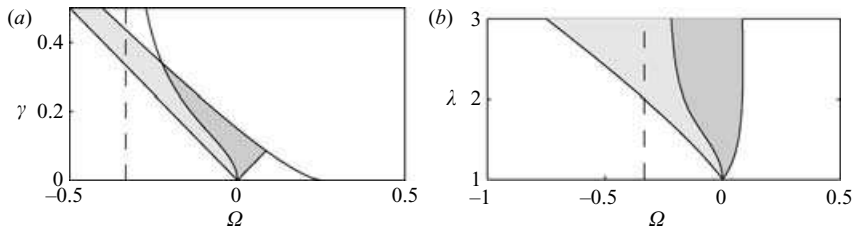

FIGURE 5. Ultra-long-wavelength stability domains in the (*a*) Ω–γ and (*b*) Ω–λ parameter spaces, for azimuthal mode $m=1$ and for $Ro=-3$. The unstable domain in the two-dimensional case is shaded. Three-dimensional effects are stabilizing in the light shaded area and destabilizing in the heavy shaded area. The dashed line shows the critical value $\Omega = 1/Ro$.

where $\ln\kappa = \ln(k|\tilde{\beta}|(\lambda+1)/4) + C - 1/4$ and the parameters Γ_i are defined in Appendix B.

When $k=0$, we recover the two-dimensional result $\sigma^2 = \gamma^2 - \Omega^2$. At leading order in k, we can replace σ^2 by its value for $k=0$ and keep only the leading $k^2\ln k$ and k^2 terms. This yields

$$\sigma^2 = \gamma^2 - \Omega^2 + \frac{\lambda}{2}\left(2\gamma^2\alpha_1 - \frac{\Omega}{Ro^2}\right)k^2\ln\kappa + 2k^2\left(\gamma\Gamma_3 - \Omega\Gamma_2 + \Gamma_1(\gamma^2-\Omega^2) - \frac{\lambda}{4Ro^2}\sqrt{\gamma^2-\Omega^2}\,\arg\tilde{\beta}\right). \quad (3.51)$$

In the ultra long-wavelength limit, the $O(k^2\ln k)$ term is dominant and we see that three-dimensional effects can be destabilizing or stabilizing if the coefficient $\mu = 2\gamma^2\alpha_1 - \Omega Ro^{-2}$ is negative or positive, respectively. The critical curve $\mu = 0$ is displayed in figure 5. The heavy and light shaded areas show the domains where three-dimensional effects are destabilizing and stabilizing, respectively. For small strain (implying small ellipticity), the critical curve $\mu = 0$ is always tangent to the γ-axis at the origin so that three-dimensional effects are destabilizing when $\Omega > 0$ and stabilizing when $\Omega < 0$, independent of Rossby number. Physically, this means that the $m = 1$ instability is three-dimensional when the angle between the major axis of the ellipse and the strain axis at infinity is larger than $\pi/4$ (figure 2*c*), and two-dimensional if it is smaller than $\pi/4$ (figure 2*b*). This can be explained partially by the fact that the self-induced frequency (three-dimensional term added to Ω in the second bracketed term of (3.50)) is in the co-rotating sense with respect to the vortex and is therefore opposite to Ω (because Ω is taken positive when the vorticity is negative). Since the background rotation Ω is stabilizing, the self-induced rotation therefore diminishes this stabilizing effect when $\Omega > 0$ and increases it when $\Omega < 0$. This is opposite to the case of a homogeneous fluid (no rotation and stratification) for which the self-induced velocity gives a counter-rotation (Moore & Saffman 1971). It would be interesting to investigate this difference by varying the stratification in addition to the rotation, but this is left for future work.

For larger strain or ellipticity, the destabilizing domain widens or shrinks if Ro is negative or positive, respectively. Beyond the critical value $Ro\Omega > 1$, three-dimensional effects are always stabilizing. This value corresponds to a critical Rossby number based on the background vorticity of $Ro_s = -\Omega/\Omega_b = -2$ (there is a minus sign because Ω is taken as positive when the vorticity is negative). However, the crucial

point is that the curve $\mu = 0$ never crosses the boundaries of the two-dimensional unstable domain in the (Ω, λ)-plane for moderate aspect ratio (figure 5*b*). This means that, independent of the Rossby number, the instability is two-dimensional for elliptical vortices when $-\gamma < \Omega < \Omega_c$, while the instability is three-dimensional, when $\Omega_c < \Omega < \gamma$, where Ω_c is the critical value of Ω corresponding to $\mu = 0$. As explained previously, this threshold is $\Omega_c \approx 0$ and only weakly depends on the Rossby number when $\lambda - 1 = O(1)$.

This is confirmed in figure 6 which shows growth rate contours obtained from the full dispersion relation (3.50) for $\lambda = 1.25$ as a function of Ω and k for various Rossby numbers. We see that the unstable domain for $k = 0$ is enclosed in the range $-0.069 < \Omega < 0.044$. This corresponds to the critical values where $\Omega = -\gamma$ and $\Omega = \gamma$ for $\lambda = 1.25$. Then, as k increases, the unstable region is shifted towards positive values of Ω, for all Rossby numbers. Therefore, when $\Omega < -\gamma$, the vortex is stable to all disturbances. In the intermediate range, $-\gamma < \Omega < \gamma$, the vortex is most unstable to two-dimensional disturbances when $\Omega < \Omega_c$ and to long-wavelength three-dimensional disturbances when $\Omega > \Omega_c$ (where $\Omega_c \approx 0$). As mentioned by Miyazaki *et al*. (1997), this means that a vortex embedded in a simple shear such that $\Omega = -\gamma$ (streamlines at infinity parallel to the major-axis of the ellipse) is stable, whereas if $\Omega = \gamma$ (streamlines at infinity perpendicular to the major-axis of the ellipse), the vortex is unstable to long-wavelength three-dimensional disturbances. Finally, for $\Omega > \gamma$, the vortex is most unstable to short-wavelength three-dimensional disturbances. When the Rossby number is decreased, this picture remains valid for small wavenumber although the unstable region is more and more bent towards positive values of Ω (the reversal of the unstable domain towards negative Ω for large wavenumber in figures 6(*a*) and 6(*d*) is probably spurious since the present asymptotic approach is valid only for small wavenumbers k). As illustrated in figure 7 for the particular case $\Omega = \gamma$, the most amplified wavenumber is proportional to the Rossby number for small Rossby number and becomes independent of the Rossby number for $Ro \to \infty$. For intermediate Rossby numbers and relatively large wavenumbers $k = O(1)$, an asymmetry can be seen between positive and negative Rossby numbers: the maximum growth rate and most amplified wavenumber are slightly larger for anticylones. This asymmetry, which is also seen in figure 6, still persists for $Ro = \pm 15$, but disappears for larger values of Ro. The above scaling corresponds to a scaling for the typical dimensional wavenumber $\hat{k} = kN/(\zeta b)$ going from $\hat{k} = O(N/(\zeta b))$ for $Ro = \infty$ to $\hat{k} = O(NRo/(\zeta b)) = O(N/(2\Omega_b b))$ for $Ro \to 0$. However, this evolution is continuous and the overall shape of the unstable domains in figure 6 do not change with the Rossby number. Practically, this means that if there is a three-dimensional instability in the quasi-geostrophic case for a given parameter set (λ, Ω) characterizing the basic flow, a similar instability will also be found for these parameters for any other value of the Rossby number, even if the maximum growth rate and most amplified wavelength differ.

Let us now look in more detail at the two limits of small and large Rossby number. In the quasi-geostrophic limit $Ro \ll 1$, or more precisely $Ro \ll 1/\gamma$ (implying $Ro \ll 1/\Omega$), we have $\mu = -\Omega/Ro^2$ so that, as in the case of small ellipticity described above, long-wavelength three-dimensional effects are destabilizing if $\Omega > 0$ and stabilizing if $\Omega < 0$. In this limit of small Rossby number, (3.50) becomes

$$\sigma^2 + \left(\Omega + \frac{\lambda k^2}{4Ro^2}\left[\ln\left(\frac{k(\lambda+1)}{4Ro}\right) + C - \tfrac{1}{4}\right]\right)^2 = \left(\gamma + \frac{(\lambda-1)\lambda}{8(\lambda+1)}\frac{k^2}{Ro^2}\right)^2. \qquad (3.52)$$

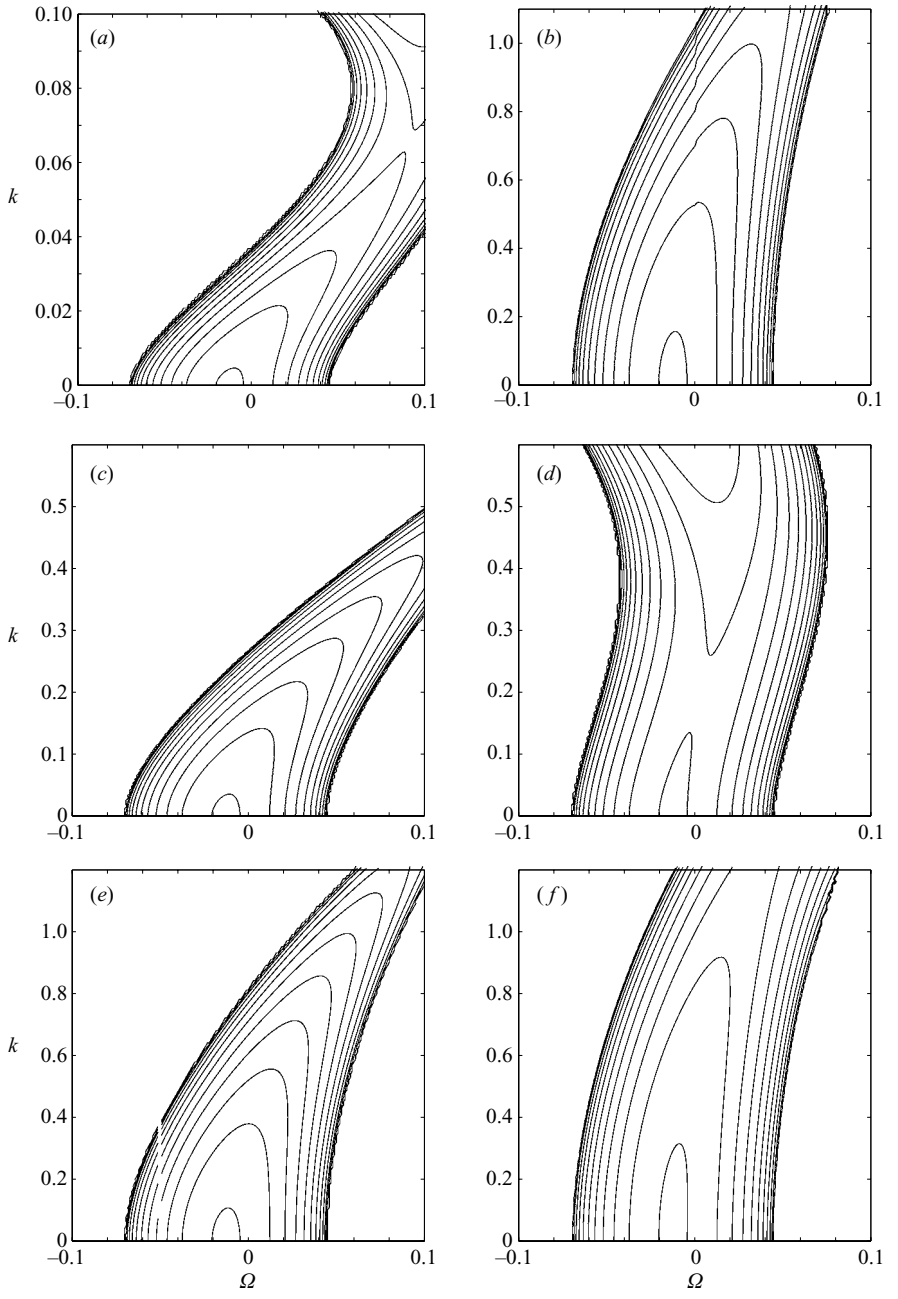

FIGURE 6. Growth rate of the azimuthal mode $m = 1$ given by (3.50) for $\lambda = 1.25$ as a function of Ω and the vertical wavenumber k for various Rossby numbers: (*a*) $Ro = 0.1$, (*b*) $Ro = \infty$, (*c*) $Ro = 1$, (*d*) $Ro = -1$, (*e*) $Ro = 10$, (*f*) $Ro = -10$. The contour interval is 0.005. Note that the y axis scale is not the same for each plot. The present asymptotic approach is valid only for small wavenumbers k and the reversal of the unstable domain towards negative Ω for large wavenumbers in (*a*) and (*d*) is probably spurious.

It is noteworthy that this dispersion relation in the limit $\lambda \to 1$ is in quantitative agreement with the quasi-geostrophic and weak ellipticity result of Dritschel (2002):

$$\sigma^2 = \gamma^2 - \left(\Omega - \tfrac{1}{2} + I_1(\tilde{k})K_1(\tilde{k})\right)^2 \approx \gamma^2 - \left[\Omega + \tfrac{1}{4}\tilde{k}^2\left(\ln\left(\tfrac{1}{2}\tilde{k}\right) + C - \tfrac{1}{4}\right)\right]^2, \qquad (3.53)$$

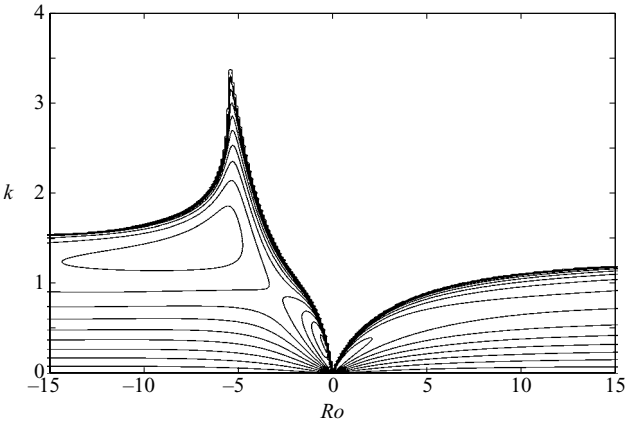

FIGURE 7. Growth rate of the azimuthal mode $m = 1$ given by (3.50) for $\lambda = 1.25$ and $\Omega = \gamma = 0.0444$ as a function of Ro and the vertical wavenumber k. The contour interval is 0.005.

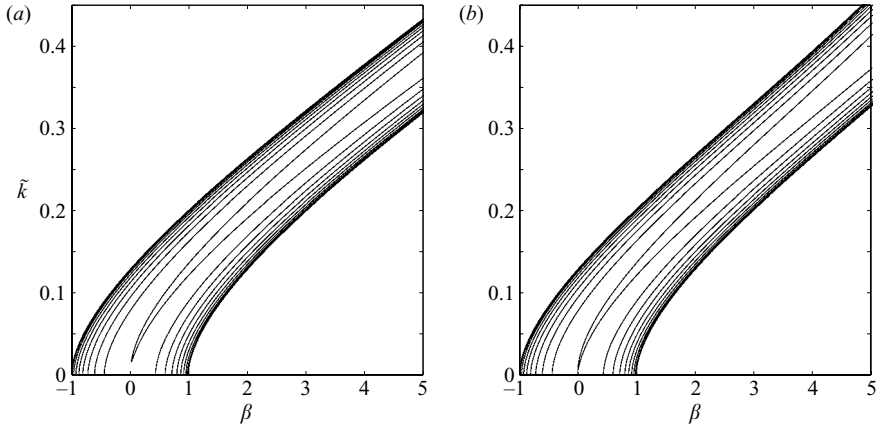

FIGURE 8. Growth rate σ/γ of the azimuthal mode $m = 1$ for $\gamma = 0.01$ (and for the basic solution with the smallest aspect ratio) as a function of $\beta = \Omega/\gamma$ and the vertical wavenumber $\tilde{k} = k\sqrt{\lambda}/Ro$. The exact result, obtained by Dritschel (2002) is shown in (a), while the asymptotic result given by (3.52) is shown in (b). The contour interval is 0.1.

where $\tilde{k} = k\sqrt{\lambda}/Ro$ owing to a different scaling for the wavenumber in Dritschel (2002). Figure 8 compares the growth rate given by (3.52) for $\gamma = 0.01$ to the exact quasi-gesotrophic results obtained numerically by Dritschel (2002). We see that the agreement is very good, even for wavenumbers with $\tilde{k} = k\sqrt{\lambda}/Ro = O(1)$, whereas the present asymptotic analysis was expected to be valid only for small wavenumbers. In particular, it is worth emphasizing that the asymptotic growth rate (3.52) is able to quantitatively predict the short-wavelength instability band for $\Omega > \gamma$ (figure 8). We expect that the agreement will continue to be good for other values of the Rossby number, but no numerical results outside the quasi-geostrophic regime are available yet. Furthermore, we note that the asymptotic growth rate (3.52) captures the increase of maximum growth rate, improving the small ellipticity result (3.53) which predicts a constant maximum growth rate. This increase is due to the last term of (3.52) which tends to increase the strain γ. As pointed out by Miyazaki *et al*. (1997), this increase is absent in homogeneous fluids (no stratification and no rotation): indeed,

the asymptotic formula of Moore & Saffman (1971) and Robinson & Saffman (1984) in the case of a pure strain ($\Omega = 0$) predicts that the maximum growth rate is equal to γ and reached for $k = 0$. In the case of a quasi-geostrophic fluid and $\Omega = 0$, (3.52) shows that the instability is slightly three-dimensional because of this effect.

The opposite limit of a strongly stratified fluid with weak planetary rotation, i.e. when $Ro \gg 1/\Omega$, is qualitatively similar to the quasi-geostrophic limit because $\mu = -2\Omega\gamma^2$. Thus, three-dimensional effects are also always destabilizing if $\Omega > 0$ and stabilizing if $\Omega < 0$. The case $\Omega = 0$ and $Ro = \infty$ is peculiar because the $O(k^2 \ln k)$ term is identically zero. Indeed, in this case, (3.50) becomes

$$\sigma^2(1-\Gamma_1 k^2)^2 + \left[\frac{\lambda k^2}{4}(\gamma^2-\sigma^2)\left(\ln\left(k\sqrt{|\sigma^2-\gamma^2|}\frac{(\lambda+1)}{4}\right)+C-\tfrac{1}{4}\right)+\Gamma_2 k^2\right]^2 = (\gamma+\Gamma_3 k^2)^2, \tag{3.54}$$

giving at leading order in k

$$\sigma^2 = \gamma^2 + 2k^2\gamma(\Gamma_3+\Gamma_1\gamma). \tag{3.55}$$

The factor $\gamma(\Gamma_3 + \Gamma_1\gamma)$ is negative regardless of λ, so long-wavelength effects are always stabilizing. It is also worth pointing out that $\Gamma_2 = -1/32$ and $\Gamma_3 = 0$ in the limit $\lambda = 1$ (implying $\gamma = 0$), so (3.54) becomes $\sigma^2 = -(k^2/32)^2$ at leading order. This is the frequency of the slow bending wave of a circular vortex in a strongly stratified fluid.

In summary, the existence and two- or three-dimensional character of the $m = 1$ instability for a given elliptical Moore–Saffman vortex in a strongly stratified rotating fluid does not depend on the Rossby number, although the wavelength and growth rate of the instability do. This indicates that the tall-column instability exists also in a strongly stratified non-rotating fluid and suggests that it might be related to the zigzag instability since these two instabilities involve vortex bending.

3.3. *Long-wavelength instability of the $m = 2$ mode*

We next treat the case of the $m = 2$ azimuthal mode. In this case, it can be shown that non-trivial terms involving the logarithm of the wavenumber only show up at order $k^4 \ln k$. Therefore a regular expansion of the perturbation inside and outside the elliptical patch is valid up to order k^2,

$$\tilde{\boldsymbol{u}}_h = \tilde{\boldsymbol{u}}_{h0} + k^2\tilde{\boldsymbol{u}}_{h2} + \cdots, \tag{3.56}$$

$$\tilde{P} = \tilde{P}_0 + k^2\tilde{P}_2 + \cdots, \tag{3.57}$$

$$\tilde{\chi} = \tilde{\chi}_0 + k^2\tilde{\chi}_2 + \cdots, \tag{3.58}$$

$$\tilde{\psi} = k^2\tilde{\psi}_2 + \cdots, \tag{3.59}$$

where the potential at order zero is

$$\tilde{\chi}_{i0} = A\cosh 2\xi\cos 2\eta + B\sinh 2\xi\sin 2\eta \quad \text{for} \quad \xi < \xi_0, \tag{3.60}$$

$$\tilde{\chi}_{o0} = \mathrm{e}^{-2\xi}(C_o\cos 2\eta + D_o\sin 2\eta) \quad \text{for} \quad \xi > \xi_0. \tag{3.61}$$

The analysis follows closely that performed for the $m = 1$ mode in § 3.2.1. Inserting the expansions (3.57)–(3.59) into the linearized equations for $F_h = 0$, (2.18), (2.26) and (2.27) allows us to determine the $O(k^2)$ perturbation fields.

The pressure at order zero is first obtained from (3.16) in the interior and the exterior of the ellipse

$$\tilde{P}_{i0} = (-\sigma A + B(Ro^{-1} + 2\Omega))\cosh 2\xi \cos 2\eta - (\sigma B + A(Ro^{-1} + 2\Omega))\sinh 2\xi \sin 2\eta + B\left(\frac{\lambda - 1}{\lambda + 1} + 2\gamma\right)(\cosh 2\xi + \cos 2\eta) - B(1 - 2\Omega) \quad \text{for} \quad \xi < \xi_0, \tag{3.62}$$

$$\tilde{P}_{o0} = -\frac{2D_o f(\xi)}{c^2} - (\sigma C_o \mathrm{e}^{-2\xi} + D_o g(\xi))\cos 2\eta - (\sigma D_o \mathrm{e}^{-2\xi} - C_o g(\xi))\sin 2\eta - \frac{f(\xi)}{h^2}(C_o \sin 2\eta - D_o \sinh 2\xi) \quad \text{for} \quad \xi > \xi_0, \tag{3.63}$$

where $g(\xi) = (Ro^{-1} + 2\Omega)\,\mathrm{e}^{-2\xi} + 2\gamma$ and we recall that $f(\xi) = -\lambda\,\mathrm{e}^{-2\xi} + c^2(\Omega + \gamma\cosh 2\xi)$.

The streamfunction ψ_2 is next obtained from (3.20),

$$\tilde{\psi}_{i2} = \psi_{i20}(\xi) + (c_1 A + c_2 B)\cosh 4\xi \cos 2\eta + (-3c_1 A + c_3 B)\cos 2\eta - (c_2 A - c_1 B)\sinh 4\xi \sin 2\eta + \psi_{i24c}(\xi)\cos 4\eta + \psi_{i24s}(\xi)\sin 4\eta, \tag{3.64}$$

$$\tilde{\psi}_{o2} = \psi_{o20}(\xi) + (U_1(\xi)C_o + U_2(\xi)D_o)\cos 2\eta + (U_1(\xi)D_o - U_2(\xi)C_o)\sin 2\eta + \psi_{o24c}(\xi)\cos 4\eta + \psi_{o24s}(\xi)\sin 4\eta, \tag{3.65}$$

where only the coefficients (c_1, c_2, c_3) and the functions U_1 and U_2 will be required in the following. They are given in Appendix C. Then, the potential $\tilde{\chi}_2$ is obtained from (3.23)

$$\tilde{\chi}_{i2} = \chi_{i20}(\xi) + (d_1 A + d_2 B)\cosh 4\xi \cos 2\eta + (d_4 A + d_5 B)\cos 2\eta - (d_2 A - d_3 B)\sinh 4\xi \sin 2\eta + \chi_{i24c}(\xi)\cos 4\eta + \chi_{i24s}(\xi)\sin 4\eta, \tag{3.66}$$

$$\tilde{\chi}_{o2} = \chi_{o20}(\xi) + (V_1(\xi)C_o + V_2(\xi)D_o)\cos 2\eta + (V_1(\xi)D_o - V_2(\xi)C_o)\sin 2\eta + \chi_{o24c}(\xi)\cos 4\eta + \chi_{o24s}(\xi)\sin 4\eta + \cdots. \tag{3.67}$$

The coefficients $(d_1, d_2, d_3, d_4, d_5)$ and the functions V_1 and V_2 are given in Appendix C. Note that the exterior potential (3.67) has been solved as an infinite Fourier series like (3.25) for $m = 1$.

At this stage, we have determined the complete solution up to order k^2, and we can now apply the boundary conditions (2.29)–(2.30)–(2.33) for the azimuthal components $\cos 2\eta$ and $\sin 2\eta$. A lengthy but straightforward calculation leads to the following dispersion relation valid up to order k^2

$$\sigma^2(1 + \Lambda_1 k^2)^2 = \frac{1}{4}\left(\frac{\lambda - 1}{\lambda + 1}\right)^4 (1 + \Lambda_3 k^2)^2 - \left(2\Omega_e - \tfrac{1}{2} + \Lambda_2 k^2\right)^2, \tag{3.68}$$

where the coefficients $(\Lambda_1, \Lambda_2, \Lambda_3)$ depend on λ, γ and Ro. Their full expressions are given in Appendix C.

At leading order in k, we can replace σ^2 by its value for $k = 0$ and keep only the leading k^2 term

$$\sigma^2 = \frac{1}{4}\left(\frac{\lambda - 1}{\lambda + 1}\right)^4 - \left(2\Omega_e - \tfrac{1}{2}\right)^2 + \mu k^2, \tag{3.69}$$

where

$$\mu = 2\left[\Lambda_1\left(2\Omega_e - \tfrac{1}{2}\right)^2 - \Lambda_2\left(2\Omega_e - \tfrac{1}{2}\right) + \frac{\Lambda_3 - \Lambda_1}{4}\left(\frac{\lambda - 1}{\lambda + 1}\right)^4\right]. \tag{3.70}$$

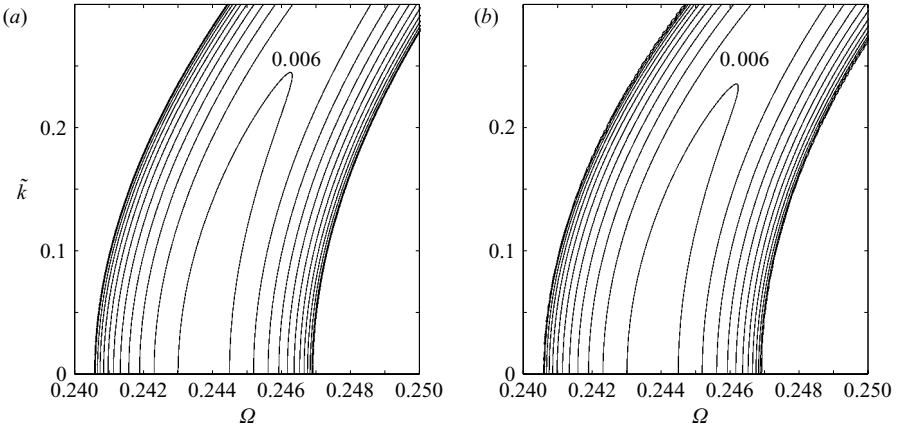

FIGURE 9. Growth rate of the azimuthal mode $m = 2$ for $\lambda = 1.25$ as a function of Ω and the vertical wavenumber $\tilde{k} = k\sqrt{\lambda}/Ro$. The exact result, obtained via the analysis described in Dritschel & de la Torre Juárez (1996) is shown in (*a*), while the asymptotic result given by (3.68) for $Ro \to 0$ is shown in (*b*). The contour interval is 0.0005.

It is instructive to first study the case of a weakly elliptical vortex, i.e. ($\lambda \approx 1$). In this limit, the mode $m = 2$ is unstable in the two-dimensional case only for very small strain $\gamma < (\lambda - 1)^3/8$ as seen from (3.5). In addition, in this limit, Ω_e is close to 1/4 so that

$$2\Omega_e - \tfrac{1}{2} \approx -(\lambda - 1)^2/8 + 2\gamma/(\lambda - 1) = O(\lambda - 1)^2 \ll 1. \tag{3.71}$$

Thus, we obtain

$$\mu \approx -(4\Omega_e - 1)\,\Lambda_2, \tag{3.72}$$

where

$$\Lambda_2 \approx \frac{1}{12}\left[\left(\frac{1}{Ro} + \frac{1}{8}\right)^2 + \frac{7}{64}\right]. \tag{3.73}$$

Because Λ_2 is positive regardless of the Rossby number, (3.72) shows that weak three-dimensional effects are always destabilizing when $\Omega_e < 1/4$ (i.e. $\gamma < \gamma_c \equiv (\lambda - 1)^3/16$ or equivalently $\Omega > \Omega_c \equiv 1/4 - (\lambda - 1)^2/8$)) and stabilizing when $\Omega_e > 1/4$ (i.e. $\gamma > \gamma_c$ or $\Omega < \Omega_c$). Most strikingly, there is no critical Rossby number for which the effect of long-wavelength $m = 2$ perturbations are reversed. The instability will be two-dimensional for $\Omega < \Omega_c$ and three-dimensional for $\Omega > \Omega_c$, independent of the Rossby number. The problem is entirely controlled by the elliptical vortex itself as for $m = 1$ – the planetary rotation plays no essential role in the instability.

In the simple case of a weakly elliptical Kirchhoff vortex, $\gamma = 0$, and in the quasi-geostrophic limit $Ro \to 0$, (3.69) reduces to $\sigma^2 = k^2(\lambda - 1)^2/48Ro^2$ in agreement with the results of Miyazaki & Hanazaki (1994) obtained by an asymptotic analysis for small ellipticity. They have interpreted this instability physically as a Benjamin–Feir instability of the $m = 2$ elliptical wave, but an alternative interpretation in terms of breaking of the rotational invariance could also be given.

Also in the quasi-geostrophic limit but now for non-zero strain and finite ellipticity, our asymptotic results are in good agreement with the numerical results of Dritschel & de la Torre Juárez (1996) and Miyazaki *et al*. (1997). As an example, figure 9 shows the contours of constant growth rate in the (Ω, $\tilde{k}$)-plane for $\lambda = 1.25$ given by (3.68) and obtained numerically by Dritschel & de la Torre Juárez (1996). The

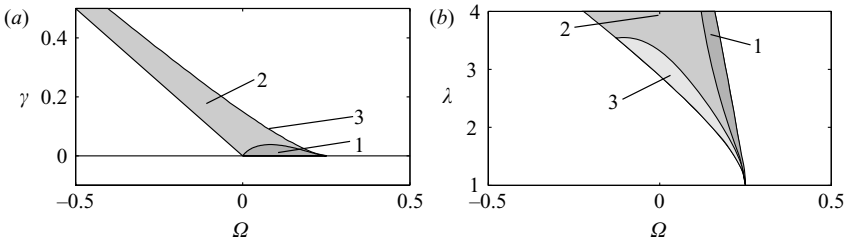

FIGURE 10. Long-wavelength stability domain in the (*a*) Ω–γ and (*b*) Ω–λ parameter spaces, for azimuthal mode $m = 2$. The unstable domain in the two-dimensional case is shaded. Weak three-dimensional effects are destabilizing in region 1 (heavy shaded) and stabilizing in region 3 (light shaded) independent of the Rossby number. In region 2 (mildly shaded), three-dimensional effects are stabilizing or destabilizing depending on the Rossby number. Note that region 3 is nearly invisible in (*a*) because it is very close to the upper limit of the two-dimensional unstable domain.

agreement is quantitatively very good even for finite values of the wavenumber. We see that three-dimensional effects tend to shift the unstable Ω-band towards positive values of Ω like for $m = 1$.

In the general case of arbitrary ellipticity, we can first study the sign of μ given by (3.70) by rewriting it in the form

$$\mu = \frac{S_2}{Ro^2} + \frac{S_1}{Ro} + S_0, \tag{3.74}$$

where the coefficients (S_2, S_1, S_0) depend only on λ and γ and can be easily obtained from $(\Lambda_1, \Lambda_2, \Lambda_3)$ (Appendix C). Figures 10(*a*) and 10(*b*) show the region where the determinant $\Delta = S_1^2 - 4S_0S_2$ is positive or negative. Region 2 corresponds to the domain where it is positive, implying that there exist two critical Rossby numbers where the sign of three-dimensional effects changes. In regions 1 and 3, the determinant is negative implying that three-dimensional effects are always destabilizing in region 1 and always stabilizing in region 3 regardless of the Rossby number. Region 1, where three-dimensional twisting effects are always destabilizing, is found principally for basic flows having an exterior elliptic background straining flow at right angles to the central elliptical vortex (figure 2*d*).

In agreement with the conclusion drawn above for small ellipticity, we see in figure 10(*b*) that region 2, where three-dimensional effects depend on the Rossby number, shrinks as $\lambda \to 1$ and widens as λ increases. For moderate values of the aspect ratio $\lambda < 3.5$, this region 2 is enclosed between regions 1 and 3. Therefore, as for the azimuthal mode $m = 1$, the unstable region in the (Ω, k)-plane will always be bent towards positive Ω when the vertical wavenumber increases regardless of the Rossby number. Figure 11 shows the complete growth rate contours in the (Ω, k)-plane computed from (3.68) for $\lambda = 1.25$ and for various Rossby numbers. We see that, indeed, the unstable domain has the same shape whatever the Rossby number. In particular, note that the case $Ro = 1$ (figure 11*c*), for which the sign of three-dimensional effects are reversed for intermediate values of Ω according to figure 10(*b*), is nevertheless similar to the other Rossby numbers. Therefore, the same conclusion as for azimuthal mode $m = 1$ holds for $m = 2$: the two- or three-dimensional character of the $m = 2$ instability is independent of the Rossby number. This means that if a long-wavelength $m = 2$ instability exists in a quasi-geostrophic fluid, this instability also exists in a strongly stratified fluid with arbitrary rotation.

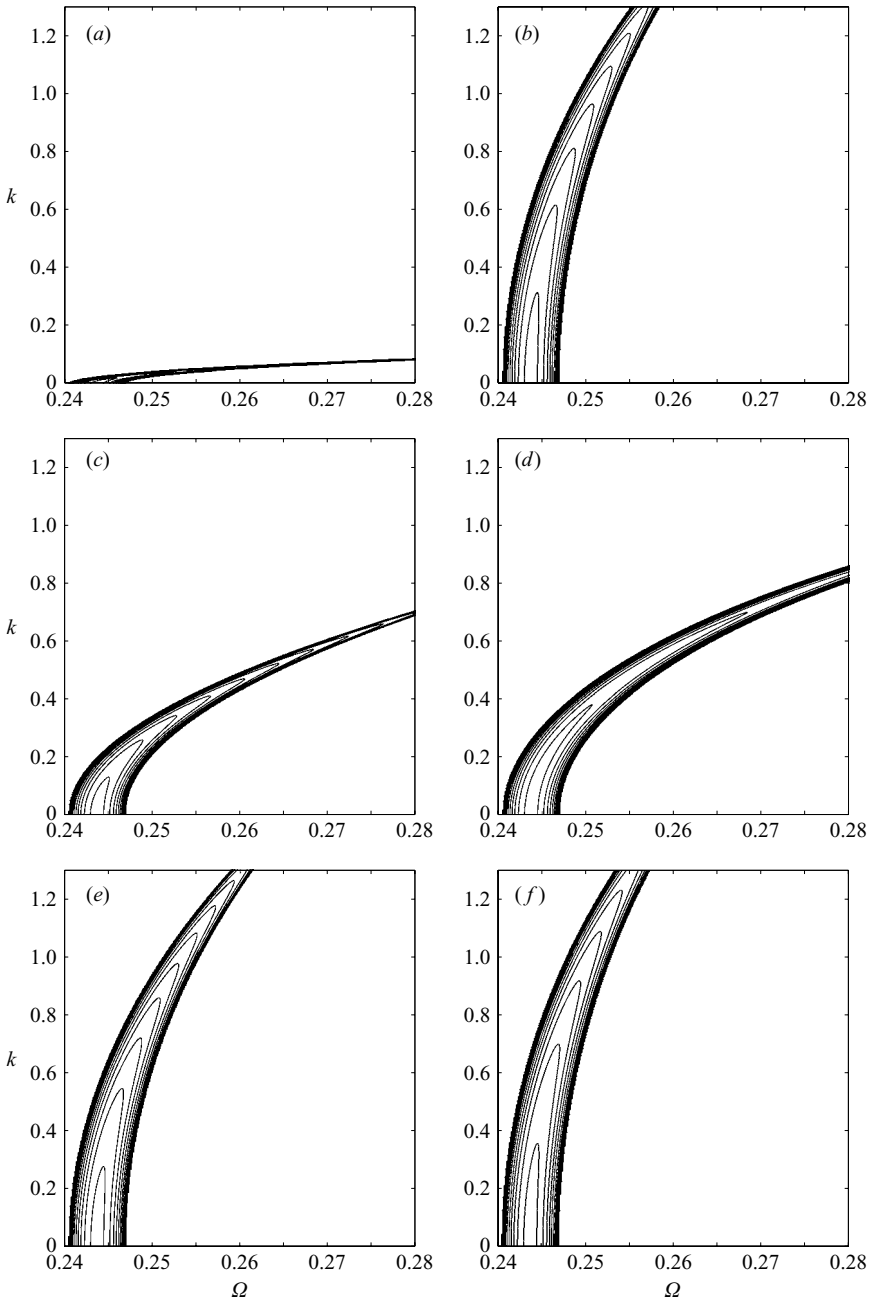

FIGURE 11. Growth rate of the azimuthal mode $m = 2$ given by (3.68) for $\lambda = 1.25$ as a function of Ω and the vertical wavenumber k for various Rossby numbers: (*a*) $Ro = 0.1$, (*b*) $Ro = \infty$, (*c*) $Ro = 1$, (*d*) $Ro = -1$, (*e*) $Ro = 10$, (*f*) $Ro = -10$. The contour interval is 0.0005.

4. Conclusions

In this paper, we have investigated the three-dimensional stability of the Moore–Saffman elliptical vortex in a strongly stratified rotating fluid by means of an asymptotic approach valid for long vertical wavelengths and negligible Froude

numbers. This basic flow is an elliptical patch of uniform vorticity surrounded by an elliptic or hyperbolic straining flow.

The main purpose of this study was to determine whether or not the three-dimensional stability properties of the Moore–Saffman vortex are significantly modified when the Rossby number is varied between the two extremes corresponding to a strongly stratified non-rotating fluid and a quasi-geostrophic (strongly stratified and rapidly rotating) fluid.

The answer is definitely no. We have seen that the Rossby number has no effect on the domains of existence for both the bending three-dimensional instability ($m = 1$) and the twisting three-dimensional instability ($m = 2$). This means that if a long-wavelength instability exists for a particular elliptical vortex in a quasi-geostrophic fluid, a similar instability should be observed for any other Rossby number, even if the detailed characteristics of the instability vary. In particular, the most amplified dimensional wavelength scales as $\zeta b/N$ when $Ro = \infty$ whereas it scales as $2\Omega_b b/N$ when $Ro \to 0$ where Ω_b is the planetary rotation. In other words, the present results indicate that the three-dimensional instabilities observed in strongly stratified fluids and quasi-geostrophic fluids are of the same physical nature.

Regarding the $m = 1$ bending instability, these results suggest that the tall-column instability observed in quasi-geostrophic fluids by Dritschel & de la Torre Juárez (1996) and the zigzag instability observed in strongly stratified fluids by Billant & Chomaz (2000*a–c*) are fundamentally related – they both involve bending of vortex columns.

Vortices in Nature such as Jupiter's Great Red Spot, the Earth's Stratospheric Polar Vortex and ocean eddies are three-dimensional in structure, and in particular have a limited vertical extent (cf. Tychensky & Carton 1998; Cho *et al*. 2001; Scott & Dritschel 2005). What our analysis suggests is that the instability found limits the height : width aspect ratio of vortices in general rotating stably stratified fluids. Not surprisingly then, we will hardly ever find 'tall' vortices to serve as candidates for our stability analysis. On the other hand, results in Dritschel *et. al.* (1999) show that two-dimensional interactions in a three-dimensional quasi-geostrophic fluid of fixed height H first make smaller two-dimensional vortices, with larger height:width aspect ratios. These smaller vortices then break down as predicted from our analysis, while larger vortices remain approximately two-dimensional. This is a beautiful example of how two-dimensional interactions can cascade to three-dimensional, producing smaller vortices from larger ones.

The present approach is restricted to long-wavelength perturbations in order to make analytical progress. Despite this limitation, we emphasize that the asymptotic results are in excellent agreement with the exact results which are available for quasi-geostrophic fluids, even for relatively large wavenumbers. To go further, and also consider the nonlinear effects of these instabilities, direct numerical simulation appears necessary. This is left for future work. Given the large number of parameters in the problem (γ, Ω, k, Ro, F_h), our asymptotic analysis should prove useful for such numerical investigations.

Appendix A. Background straining flow (2.7)

In order to illustrate how the background flow (2.7) can arise, we consider in this Appendix the example of two distant vortices of relative circulations $2\pi\kappa_1$ and $2\pi\kappa_2$ separated by a distance d in the planetary frame of reference rotating at rate Ω_b. We suppose that the vortices are compact (i.e. patches) with a radius R much less than

d. Then, the relative vorticity outside the vortex cores is zero and for example, the velocity of the first vortex induced on the other is $\boldsymbol{u_1} = (\kappa_1/r)\boldsymbol{e}_\theta$ where (r, θ) are the cylindrical coordinates centred on the first vortex. At leading order in R/d, the second vortex is therefore advected at the constant velocity $\boldsymbol{u_1} = (\kappa_1/d)\boldsymbol{e}_\theta$ which combined with the velocity induced by the second vortex on the first, causes the vortices to rotate steadily around each other at rate $\Omega = (\kappa_1+\kappa_2)/d^2$. The rotation axis is located on the line connecting the two vortices at a distance $d_2 = \kappa_1 d/(\kappa_1 + \kappa_2)$ from the centre of vortex 2 (toward vortex 1). If we go into a frame of reference rotating at rate $\Omega_b + \Omega$ relative to the absolute reference frame, the vortex pair is steady and the flow field in the vicinity of the second vortex becomes

$$\boldsymbol{u_1}' = \frac{\kappa_1}{(d+x)^2+y^2}(-y\boldsymbol{e}_x + (d+x)\boldsymbol{e}_y) - \Omega(-y\boldsymbol{e}_x + (x+d_2)\boldsymbol{e}_y),$$

where (x, y) are the Cartesisan coordinates centred on the second vortex. When the distance d is large: $d \gg (x, y)$, this approximates to

$$\boldsymbol{u_1}' = -\frac{\kappa_1}{d^2}(y\boldsymbol{e}_x + x\boldsymbol{e}_y) - \Omega(-y\boldsymbol{e}_x + x\boldsymbol{e}_y) + O(x^2/d^3, y^2/d^3),$$

which has the form (2.7) with $\gamma = \kappa_1/d^2$.

Appendix B. Coefficients and functions for the $m = 1$ mode

The coefficients introduced in (3.21) are

$$a_1 = -\frac{c^2\sigma}{8}\left(\frac{1}{Ro}+1\right), \tag{B 1}$$

$$a_2 = \frac{c^2}{8}\left(\frac{1}{Ro}+1\right)\left(\frac{1}{Ro}+\Omega+\gamma+\frac{\lambda}{\lambda+1}\right), \tag{B 2}$$

$$a_3 = -\frac{c^2}{8}\left(\frac{1}{Ro}+1\right)\left(\frac{1}{Ro}+\Omega-\gamma+\frac{1}{\lambda+1}\right). \tag{B 3}$$

The functions introduced in (3.22) are

$$H_1 = -\frac{c^2\sigma}{32Ro}(\mathrm{e}^{-3\xi} + 8\xi\cosh\xi), \tag{B 4}$$

$$H_2 = -\frac{c^2}{32Ro}\left[\left(\gamma - 2\frac{\lambda}{c^2} + \frac{1}{Ro} + \Omega\right)\mathrm{e}^{-3\xi} - 8\frac{\lambda}{c^2}\xi\mathrm{e}^{-\xi} + 8\alpha_1\xi\cosh\xi\right], \tag{B 5}$$

$$H_3 = -\frac{c^2}{32Ro}\left[\left(\gamma - 2\frac{\lambda}{c^2} - \frac{1}{Ro} - \Omega\right)\mathrm{e}^{-3\xi} + 8\frac{\lambda}{c^2}\xi\mathrm{e}^{-\xi} - 8\alpha_1\xi\sinh\xi\right], \tag{B 6}$$

$$H_4 = -\frac{c^2\sigma}{32Ro}(\mathrm{e}^{-3\xi} + 8\xi\sinh\xi). \tag{B 7}$$

The coefficients introduced in (3.24) are

$$b_1 = \frac{c^2}{8}\left[\left(\frac{1}{\lambda+1}+\frac{1}{Ro}+\Omega-\gamma\right)\left(\frac{1}{\lambda+1}-\gamma-\Omega\right)+\sigma^2\right], \tag{B 8}$$

$$b_2 = -\frac{c^2\sigma}{8}\left(\frac{1}{Ro}+2\Omega+2\gamma+\frac{\lambda-1}{\lambda+1}\right), \tag{B 9}$$

$$b_3 = \frac{c^2\sigma}{8}\left(\frac{1}{Ro}+2\Omega-2\gamma-\frac{\lambda-1}{\lambda+1}\right), \tag{B 10}$$

$$b_4 = \frac{c^2}{8}\left[\left(\frac{\lambda}{\lambda+1}+\frac{1}{Ro}+\Omega+\gamma\right)\left(\frac{\lambda}{\lambda+1}+\gamma-\Omega\right)+\sigma^2\right]. \tag{B 11}$$

The functions introduced in (3.25) are

$$G_1 = \frac{1}{24c^2}(2\lambda - \gamma c^2)^2 \cosh\xi \mathrm{e}^{-6\xi} - \frac{\Omega}{8}(2\lambda - c^2\gamma)\mathrm{e}^{-5\xi} + \frac{1}{32}\left[c^2\left(7\Omega^2 - \frac{\Omega}{Ro} + \sigma^2\right) - (2\lambda - c^2\gamma)\left(-\alpha_4 + 3\gamma + \frac{2\lambda}{c^2}\right)\right]\mathrm{e}^{-3\xi} + \frac{c^2}{4}(\sigma^2 - \gamma^2 + \Omega\alpha_1)\xi\cosh\xi + \frac{\lambda}{4}(\alpha_2 + \gamma)\xi\mathrm{e}^{-\xi}, \tag{B 12}$$

$$G_2 = \frac{\sigma}{16}\left(c^2(\gamma + \Omega) + \frac{c^2}{2Ro} - 2\lambda\right)\mathrm{e}^{-3\xi} + \frac{\sigma}{4}c^2\alpha_2\xi\cosh\xi - \sigma\frac{\lambda}{2}\xi\mathrm{e}^{-\xi}, \tag{B 13}$$

$$G_3 = \frac{\sigma}{16}\left(c^2(\gamma - \Omega) - \frac{c^2}{2Ro} - 2\lambda\right)\mathrm{e}^{-3\xi} - \frac{\sigma}{4}c^2\alpha_2\xi\sinh\xi + \sigma\frac{\lambda}{2}\xi\mathrm{e}^{-\xi}, \tag{B 14}$$

$$G_4 = -\frac{1}{24c^2}(2\lambda - \gamma c^2)^2 \sinh\xi\mathrm{e}^{-6\xi} - \frac{\Omega}{8}(2\lambda - c^2\gamma)\mathrm{e}^{-5\xi} + \frac{1}{32}\left[c^2\left(7\Omega^2 - \frac{\Omega}{Ro} + \sigma^2\right) - (2\lambda - c^2\gamma)\left(\alpha_4 + 3\gamma + \frac{2\lambda}{c^2}\right)\right]\mathrm{e}^{-3\xi} + \frac{c^2}{4}(\sigma^2 - \gamma^2 + \Omega\alpha_1)\xi\sinh\xi + \frac{\lambda}{4}(\alpha_2 - \gamma)\xi\mathrm{e}^{-\xi}. \tag{B 15}$$

The constants introduced in (3.42)–(3.43) are

$$C_2 = \frac{c^2}{4}[(\sigma^2 - \gamma^2 + \Omega\alpha_1)C_o + \sigma\alpha_2 D_o], \tag{B 16}$$

$$D_2 = \frac{c^2}{4}[(\sigma^2 - \gamma^2 + \Omega\alpha_1)D_o - \sigma\alpha_2 C_o], \tag{B 17}$$

$$C_3 = C_2\left[\ln\left(\frac{|\tilde{\beta}|c}{4}\right) + C - \tfrac{1}{2}\right] + D_2\arg\tilde{\beta}, \tag{B 18}$$

$$D_3 = D_2\left[\ln\left(\frac{|\tilde{\beta}|c}{4}\right) + C - \tfrac{1}{2}\right] - C_2\arg\tilde{\beta}, \tag{B 19}$$

$$L_2 = -\frac{c^2}{4Ro}(\sigma C_o + \alpha_1 D_o), \tag{B 20}$$

$$M_2 = -\frac{c^2}{4Ro}(\sigma D_o - \alpha_1 C_o), \tag{B 21}$$

$$L_3 = L_2\left[\ln\left(\frac{|\tilde{\beta}|c}{4}\right) + C - \tfrac{1}{2}\right] + M_2\arg\tilde{\beta}, \tag{B 22}$$

$$M_3 = M_2\left[\ln\left(\frac{|\tilde{\beta}|c}{4}\right) + C - \tfrac{1}{2}\right] - L_2\arg\tilde{\beta}. \tag{B 23}$$

The coefficients introduced in (3.50) are

$$\Gamma_1 = \frac{\lambda}{4}\left(\frac{1}{Ro} + \gamma\frac{\lambda - 1}{\lambda + 1} + \frac{1 - 3\lambda + \lambda^2}{(1 + \lambda)^2}\right), \tag{B 24}$$

$$\Gamma_2 = -\frac{\lambda}{4Ro}\left(\Omega + 3\frac{\lambda}{(\lambda + 1)^2}\right) + \sigma^2\frac{(\lambda - 1)^2}{8} + \frac{\lambda}{8(\lambda^2 + 1)^2}\left[(\lambda - 1)^2(3 - 2\lambda + 3\lambda^2)\Omega^2 + \left(8\Omega\frac{\lambda^2}{(\lambda + 1)^2} - \lambda\right)(1 - \lambda + \lambda^2)\right], \tag{B 25}$$

$$\Gamma_3 = \frac{(\lambda-1)\lambda}{8(\lambda+1)Ro^2} - \frac{(\lambda-1)\lambda^2}{4(\lambda+1)(1+\lambda^2)Ro}(1-2\Omega) + \frac{\lambda-1}{24(\lambda+1)}\left[-3(1-\lambda+\lambda^2)\sigma^2 - \frac{2\lambda}{(\lambda^2+1)^2}(1-4\lambda-4\lambda^3+\lambda^4)\Omega^2 + \frac{2\lambda^2}{(\lambda^2+1)^2}(1-\lambda)^2\Omega - \frac{\lambda^2}{(\lambda^2+1)^2}(3-\lambda+3\lambda^2)\right]. \quad \text{(B 26)}$$

Appendix C. Coefficients and functions for the $m = 2$ mode

The coefficients introduced in (3.64) are

$$c_1 = -\frac{c^2\sigma}{48}\left(\frac{1}{Ro}+1\right), \quad \text{(C 1)}$$

$$c_2 = \frac{c^2}{48}\left(\frac{1}{Ro}+2\Omega\right)\left(\frac{1}{Ro}+1\right), \quad \text{(C 2)}$$

$$c_3 = -\frac{c^2}{16}(2+\alpha_2)\left(\frac{1}{Ro}+1\right). \quad \text{(C 3)}$$

The functions introduced in (3.65) are

$$U_1 = -\frac{c^2\sigma}{48Ro}(\mathrm{e}^{-4\xi}-3), \quad \text{(C 4)}$$

$$U_2 = -\frac{1}{Ro}\left(\frac{c^2}{48Ro}(\mathrm{e}^{-4\xi}-3) - \frac{\xi}{4}\lambda\mathrm{e}^{-2\xi} + \frac{\Omega c^2}{24}(\mathrm{e}^{-4\xi}+3)\right). \quad \text{(C 5)}$$

The coefficients introduced in (3.66) are

$$d_1 = \frac{c^2}{48}\left[(1-2\Omega)\left(\frac{1}{Ro}+2\Omega\right)+\sigma^2\right], \quad \text{(C 6)}$$

$$d_2 = \frac{c^2}{48}\sigma\left(1-4\Omega-\frac{1}{Ro}\right), \quad \text{(C 7)}$$

$$d_3 = \frac{c^2}{48}\left[\sigma^2+(1-2\Omega)\left(\frac{1}{Ro}+2\Omega\right)+\left(2\gamma+\frac{\lambda-1}{\lambda+1}\right)^2\right], \quad \text{(C 8)}$$

$$d_4 = \frac{c^2}{16}\left[(1-2\Omega)\left(\frac{1}{Ro}+2\Omega\right)-\sigma^2\right], \quad \text{(C 9)}$$

$$d_5 = \frac{c^2}{16}\sigma(3+\alpha_4). \quad \text{(C 10)}$$

The functions introduced in (3.67) are

$$V_1 = \frac{c^2}{16}(2\gamma^2-\sigma^2-2\Omega\alpha_2) + \frac{\lambda}{4}\alpha_4\xi\mathrm{e}^{-2\xi} + \frac{c^2}{48}\left(\sigma^2+16\Omega^2+8\gamma^2-2\Omega\alpha_2-8\frac{\lambda}{c^4}(\gamma c^2+2\lambda)\right)\mathrm{e}^{-4\xi} - \frac{\Omega}{4}(2\lambda-c^2\gamma)\mathrm{e}^{-6\xi} + \frac{1}{24}\left(\frac{4\lambda^2}{c^2}-4\lambda\gamma+c^2\gamma^2\right)\mathrm{e}^{-8\xi}, \quad \text{(C 11)}$$

$$V_2 = \frac{c^2\sigma}{48}\left[-3\alpha_4-24\frac{\lambda}{c^2}\xi\mathrm{e}^{-2\xi}+\left(\frac{1}{Ro}+4\Omega\right)\mathrm{e}^{-4\xi}\right]. \quad \text{(C 12)}$$

The coefficients introduced in (3.68) are

$$\Lambda_1 = \frac{\lambda}{12}\left(\alpha_4 - \frac{3}{(\lambda+1)^4}(1-2\lambda-2\lambda^2-2\lambda^3+\lambda^4)\right), \tag{C 13}$$

$$\begin{aligned}\Lambda_2 = {} & \frac{1}{Ro}\left(\frac{1+\lambda^2}{24}\alpha_2 + \frac{\lambda}{8(\lambda+1)^4}(3+2\lambda^2+3\lambda^4)\right) - \frac{1+\lambda^2}{24}\sigma^2 \\ & + \gamma^2\frac{1}{12(\lambda^2-1)^2}(1+7\lambda^2+7\lambda^4+\lambda^6) \\ & + \gamma\frac{\lambda^2}{6(\lambda+1)^5(\lambda-1)}(1-8\lambda+6\lambda^2-8\lambda^3+\lambda^4) \\ & + \frac{\lambda}{24(\lambda+1)^6}(3+8\lambda-11\lambda^2+16\lambda^3-11\lambda^4+8\lambda^5+3\lambda^6),\end{aligned} \tag{C 14}$$

$$\begin{aligned}\Lambda_3 = {} & -\frac{1}{12Ro}((1+4\lambda+\lambda^2)\alpha_2+9\lambda) + \frac{(1-\lambda)^2}{12}\sigma^2 \\ & - \gamma^2\frac{1}{6(\lambda^2-1)^2}(1+4\lambda+7\lambda^2-8\lambda^3+7\lambda^4+4\lambda^5+\lambda^6) \\ & - \gamma\frac{\lambda^2}{3(\lambda+1)^3(\lambda-1)}(1-6\lambda+\lambda^2) \\ & - \frac{\lambda}{12(\lambda+1)^4}(3+14\lambda+14\lambda^2+14\lambda^3+3\lambda^4).\end{aligned} \tag{C 15}$$

REFERENCES

Billant, P. & Chomaz, J.-M. 2000*a* Experimental evidence for a new instability of a vertical columnar vortex pair in a strongly stratified fluid. *J. Fluid Mech.* **418**, 167–188.

Billant, P. & Chomaz, J.-M. 2000*b* Theoretical analysis of the zigzag instability of a vertical columnar vortex pair in a strongly stratified fluid. *J. Fluid Mech.* **419**, 29–63.

Billant, P. & Chomaz, J.-M. 2000*c* Three-dimensional stability analysis of a vertical columnar vortex pair in a stratified fluid. *J. Fluid Mech.* **419**, 65–91.

Billant, P. & Chomaz, J.-M. 2001 Self-similarity of strongly stratified inviscid flows. *Phys. Fluids* **13**, 1645–1651.

Cho, J. Y.-K., de la Torre Juárez, M., Ingersoll, A. & Dritschel, D. G. 2001 A high-resolution, three-dimensional model of Jupiter's Great Red Spot. *J. Geophys. Res. Planets* **106(E3)**, 5099–5105.

Dritschel, D. G. 2002 Vortex merger in rotating stratified flows. *J. Fluid Mech.* **455**, 83–101.

Dritschel, D. G. & de la Torre Juárez, M. 1996 The instability and breakdown of tall columnar vortices in a quasi-geostrophic fluid. *J. Fluid Mech.* **328**, 129–160.

Dritschel, D. G., Ambaum, M. H. P. & de la Torre Juárez, M. 1999 On the three-dimensional vortical nature of atmospheric and oceanic flows. *Phys. Fluids* **11**, 1512–1520.

Hinch, E. J. 1991 *Perturbation Methods.* Cambridge University Press.

Kerswell, R. R. 2002 Elliptical instability. *Annu. Rev. Fluid Mech.* **34**, 83–113.

Kida, S. 1981 Motion of an elliptic vortex in a uniform shear flow. *J. Phys. Soc. Japan* **50**, 3517–3520.

Le Dizès, S. & Eloy, C. 1999 Short-wavelength instability of a vortex in a multipolar strain field. *Phys. Fluids* **11**, 500–502.

Lindborg, E. 2002 Strongly stratified turbulence: a special type of motion. *Advances in turbulence IX, Proc. Ninth European Turbulence Conf. Southampton.*

Love, A. E. H. 1893 On the stability of certain vortex motions. *Proc. Lond. Math. Soc.* **25**, 18–42.

Miyazaki, T. 1993 Elliptical instability in a stably stratified rotating fluid. *Phys. Fluids* **5**, 2702–2709.

Miyazaki, T. & Hanazaki, H. 1994 Baroclinic instability of Kirchhoff's elliptic vortex. *J. Fluid Mech.* **261**, 253–271.

Miyazaki, T., Hirahara, K. & Hanazaki, H. 1997 The quasi-three-dimensional instability of an elliptical vortex subject to a strain field in rotating stratified fluid. *Fluid Dyn. Res.* **21**, 359–380.

Moore, D. W. & Saffman, P. G. 1971 Structure of a line vortex in an imposed strain. In *Aircraft Wake Turbulence* (ed. J. H. Olsen, A. Goldburg & M. Rogers). Plenum.

Moore, D.W. & Saffman, P.G. 1975 The instability of a straight vortex filament in a strain field. *Proc. R. Soc. Lond.* A **346**, 413–425.

Pierrehumbert, R. T. 1986 Universal short-wave instability of two-dimensional eddies in an inviscid fluid. *Phys. Rev. Lett.* **57**, 2157–2159.

Riley, J. J. & Lelong, M.-P. 2000 Fluid motions in the presence of strong stable stratification. *Annu. Rev. Fluid Mech.* **32**, 613–657.

Robinson, A. C. & Saffman, P. G. 1984 Three-dimensional stability of an elliptical vortex in a straining field. *J. Fluid Mech.* **142**, 451–466.

Scott, R. K. & Dritschel, D. G. 2005 Downward wave propagation on the polarvortex. *J. Atmos. Sci.* **62**, 3382–3395.

Tsai, C. Y. & Widnall, S. E. 1976 The stability of short waves on a straight vortex filament in a weak externally imposed strain field. *J. Fluid Mech.* **73**, 721–733.

Tychensky, A. & Carton, X. J. 1998 Hydrological and dynamical characterization of Meddies in the Azores region: a paradigm for baroclinic vortex dynamics. *J. Geophys. Res.* **103**, 25061–25079.

Waleffe, F. 1990 On the three-dimensional instability of strained vortices. *Phys. Fluids* A **2**, 76–80.